Groundwater Research Report
WR11R005

Preferential Flow Paths in Heterogeneous Glacially-Deposited Aquitards

David J Hart, Ph.D.

2013

Project Number WR11R005

Preferential Flow Paths in Heterogeneous Glacially-Deposited Aquitards

David J. Hart
Wisconsin Geological and Natural History Survey
Madison, Wisconsin

Administered by:
University of Wisconsin Water Resources Institute

Funded by:
State of Wisconsin Groundwater Research and Monitoring Program

2013

This project was also supported, in part, by General Purpose Revenue funds of the State of Wisconsin to the University of Wisconsin System for the performance of research on groundwater quality and quantity. Selection of projects was conducted on a competitive basis through a joint solicitation from the University and the Wisconsin Departments of Natural Resources; Agriculture, Trade and Consumer Protection; Commerce; and advice of the Wisconsin Groundwater Research Advisory Council and with the concurrence of the Wisconsin Groundwater Coordinating Council.

Preferential Flow Paths in Heterogeneous Glacially-Deposited Aquitards

(WRI Project Number WR11R005)

Principal Investigator: David J. Hart, Wisconsin Geological and Natural History Survey

Table of Contents

List of Figures and Tables

Title: *Preferential Flow Paths in Heterogeneous Glacially-Deposited Aquitards*

Project I.D.: WRI Project Number WR11R005

Investigators: Principal Investigator- *David J. Hart, Hydrogeologist, Wisconsin Geological and Natural History Survey, University of Wisconsin–Extension, 3817 Mineral Point Road, Madison, WI 53705*
Research Assistant- *Kallina M. Dunkle, Graduate Student, Department of Geoscience, University of Wisconsin-Madison, 1215 West Dayton Street, Madison, WI 53706*

Period of Contract: July 1, 2011- June 30, 2012

Background/Need: Preferential flow paths allow for faster movement of fluids than the surrounding matrix due to their hydraulic properties and connectivity. They are important to both groundwater flow and contaminant transport, but are difficult to detect and quantify, especially in aquitards. Preferential flow paths may be caused by fractures and lenses of sediment with high hydraulic conductivity (K) such as sand bodies within a clay matrix. Researchers have discovered that even thick aquitards (greater than 150 ft) may have fractures that are capable of transporting contaminants (Cherry *et al*., 2006; Gerber *et al*., 2001) and affecting underlying aquifers. However, few researchers have documented preferential flow paths created by connected sand lenses/bodies. Techniques to delineate preferential flow paths in aquitards are key to determining recharge to underlying confined aquifers and for protection of underlying aquifers.

This project focuses on delineating preferential flow paths in a heterogeneous glacially-deposited aquitard. A representative site has been selected in Outagamie County, Wisconsin where a bedrock valley has been filled with a thick sequence of sediment, dominated by lake sediment with some glacial till and sand lenses of uncertain deposition. This sediment appears to form an extensive aquitard comprised of very low conductivity sediment, occasionally surrounding sand lenses of unknown extent and continuity. Results of this project will be useful to both the municipal and private well owners in Outagamie County. The results can be used in a variety of ways including groundwater management such as siting municipal wells, land use planning such as siting landfills, and public information regarding Wisconsin glacial history.

Objectives: The main objective of this study was to delineate preferential flow paths using multiple-point geostatistics and groundwater flow models for a representative site in Outagamie County, Wisconsin. Additional objectives included demonstrating the use of multiple-point geostatistics, understanding the flow system in Outagamie County, and reviewing and revising the depositional history of glacial Lake Oshkosh.

Methods: Multiple-point geostatistics (Guardino & Srivastava, 1993) was used to create 300 three-dimensional hydrostratigraphic models for the representative site in Outagamie County, Wisconsin, using as input data a combination of well construction reports, electrical resistivity imaging, geoprobe sampling, and reasonable depositional histories. Multiple-point geostatistics uses training images, either 2-D or 3-D, that represent the general features of the subsurface (i.e., channels, lenses). Training images have advantages over variograms, the more traditional geostatistical approach, because training images can include soft data, such as outcrops or geophysics, and can maintain geologic structure and continuity. All 300 hydrostratigraphic models were analyzed for statistics of connectivity and a representative set of six hydrostratigraphic models was selected and imported into groundwater flow and transport models based on these analyses. The groundwater flow models were calibrated to head data, the calibration was checked with streamflow measurements, and particle tracking was performed and compared to statistics of connectivity.

Results and Discussion: Analysis of well construction reports, digital elevation models, and information on the known outlets of glacial Lake Oshkosh indicated the origin of sand and gravel deposits is most likely a combination of beach and underflow deposits, making up to 20% by volume of the total sediments. All 300 models had at least one connected high K zone in the horizontal and vertical directions (percolating pathway), as indicated by statistics of connectivity. Results of the particle tracking indicated that 6% of the particles moved through the glacial deposits and exited into the surrounding bedrock in fewer than 100 years, indicating preferential flow may be occurring. Also, examples of individual particles traced through high K units in faster time than nearby particles moving through low K units were found in every model. Analyses indicated a general lack of correlation between the particle tracking results and the statistics of connectivity. This is probably due to all of the hydrostratigraphic models being geologically plausible and well-connected; thus the statistics and particle tracking have little variation.

Conclusions/Implications/Recommendations: This is one of the first examples demonstrating the use of multiple-point geostatistics in three-dimensions with a variety of data, including surface geophysics and depositional environment information. This work demonstrates that preferential flow can occur in a glacially-deposited aquitard through connected sand bodies without the presence of fractures. Overall, results of the statistics of connectivity and particle tracking indicate that a hydrostratigraphic model with fewer, longer pathways or one with many shorter pathways can create preferential flow paths and can calibrate to head and streamflow data. Finally, preferential flow is likely occurring in glacial Lake Oshkosh sediment as indicated by the analysis of the connectivity statistics for the hydrostratigraphic models and results of the particle tracking. However, the groundwater flow models should be better calibrated in order to use them for purposes of groundwater management in Outagamie County. This will require a joint calibration of groundwater flow and transport models (with oxygen isotope data) as well as collection of additional head, stream flux, and isotope targets.

Related Publications:

1) Dunkle, K.M., Hart, D.J., and Anderson, M.P., 2013. Groundwater flow model calibration difficulties in areas with glacially-deposited aquitards: An example from glacial Lake Oshkosh, Geological Society of America *Abstracts with Programs*, vol. 45, no. 4, p. 53.

2) Dunkle, K.M., Hart, D.J., and Anderson, M.P., 2012. Preferential flow paths in glacial Lake Oshkosh sediment, Outagamie County, WI, Geological Society of America *Abstracts with Programs*, vol. 44, no. 7, p. 145.

3) Dunkle, K.M., Hart, D.J., and Anderson, M.P., 2011. Hydrostratigraphic & groundwater flow models for glacial Lake Oshkosh sediment, Outagamie County, WI, Geological Society of America *Abstracts with Programs*, vol. 43, no. 5, p.560.

4) Dunkle, K.M., Hart, D.J., and Anderson, M.P., 2011. Multiple-point geostatistics for creation of 3D hydrostratigraphic models, Outagamie County, WI, Three Dimensional Geological Mapping: Workshop Extended Abstracts, Geological Survey of Canada, Open File 6998.

Key Words: *aquitard, glacial hydrostratigraphy, glacial Lake Oshkosh, groundwater flow modeling, multiple-point geostatistics, preferential flow*

Funding: University of Wisconsin Water Resources Institute

INTRODUCTION

Preferential flow paths allow for faster movement of fluids than the surrounding matrix due to their hydraulic properties and connectivity. They are important to both groundwater flow and contaminant transport, but are difficult to detect and quantify, especially in aquitards. Preferential flow paths may be caused by fractures and lenses of sediment with high hydraulic conductivity (K) such as sand bodies within a clay matrix. Researchers have discovered that even thick aquitards (greater than 150 ft) may have fractures that are capable of transporting contaminants (Cherry *et al*., 2006; Gerber *et al*., 2001) and affecting underlying aquifers. However, few researchers have documented preferential flow paths created by connected sand lenses/bodies. Techniques to delineate preferential flow paths in aquitards are key to determining recharge to underlying confined aquifers and for protection of underlying aquifers.

The main objective of this study was to delineate preferential flow paths using multiple-point geostatistics and groundwater flow and transport models for a representative site in Outagamie County, Wisconsin. The Wisconsin Geological and Natural History Survey has done extensive work in Outagamie County to define the distribution and type of glacial deposits. As part of this work, a thick sequence of fine-grained glacial sediment consisting mainly of lake sediment and till was delineated in an east-west trending buried bedrock valley (Fig.1). Outside of this valley, the fine-grained sediment is significantly thinner but appears to drape over the bedrock surface. Given that bedrock aquifers are one of the primary resources for drinking water in Outagamie County, a groundwater investigation was conducted to identify potential recharge areas in the county (Hooyer *et al*., 2008). As part of this project four rotosonic boreholes were drilled along the axis of the valley and multilevel wells were installed in two of them (RS-17 and RS-18). Two other boreholes were also drilled where the fine-grained sediment was much thinner over bedrock (<50 ft). These boreholes, located at the Riehl and Lorenz Farms, were drilled using a hollow-stem auger. Three multilevel wells were installed in each of these boreholes. With the exception of RS-17, water Leveloggers® were installed and have continuously recorded in every well since 2007 to monitor the pressure heads in the aquitard. The RS-18 location contained a sand body at a depth of 40-60 feet, and sand bodies of similar thicknesses have been noted in multiple private well logs in the study area. Intact core samples from RS-18 and other rotosonic boreholes drilled through the fine-grained sediment were collected for consolidation testing, which determines preconsolidation stress, hydraulic diffusivity (D), and specific storage(S_s) (Grisak and Cherry, 1975; Hooyer et al., 2008). The vertical K can then be calculated from D and S_s. Slug tests performed in the wells at RS-18, Riehl, and Lorenz Farms revealed that K values range from 1×10^{-8} to 5×10^{-14} m/s for the fine-grained sediment, and 2.5×10^{-4} to 6.0×10^{-5} m/s for the sand bodies.

Pore and well water samples from RS-17, RS-18, and RS-14 were analyzed for oxygen ($\delta^{18}O$) and hydrogen ($\delta^{2}H$) isotopes and well water was analyzed for tritium and the following major ions: calcium, magnesium, potassium, sodium, chloride, bicarbonate, sulfate, nitrite, and nitrate. These wells have modern $\delta^{18}O$ values at the surface, then gradually decrease with depth (indicating older water) and then increase toward more modern values near the bedrock surface. The modern values near the bedrock surface are surprising, given that studies of stable isotope geochemistry of the Cambrian Ordovician aquifer system (Perry *et al*., 1982; Siegel and Mandle, 1984) show a significant portion of the groundwater in these aquifers may be as much as hundreds of thousands of years old. Hooyer *et al*. (2008) believe this difference in $\delta^{18}O$ values is due to recharge occurring to the bedrock aquifer where the glacial sediment is thin (<50 ft). However, recharge could be occurring through preferential flow paths such as sand lenses where the sediment is thick (~200-300 ft), allowing for faster movement of groundwater and contaminants. Thus, it is important to determine the connectedness of the sand bodies within this thick sequence of sediment.

As part of Kallina Dunkle's dissertation research approximately 2,200 Wisconsin Well Construction Reports (WCRs) with driller described lithologies were used to analyze the unconsolidated sediment. These sediments were categorized into distinct hydrofacies ranging from dominantly clay or silty clay to coarse sand or gravel. Most drillers lack formal geologic training and often subtle differences in sediment are not reflected in cuttings. Thus the quality of these data varies considerably. For example, terms such as "hardpan" usually refer to glacial till, but so can “stoney clay” or “clayey gravel”, among other designations. Considerable effort was made to be consistent and as accurate as possible in transforming the driller’s descriptions into geologic categories. Analysis of the WCRs indicated the presence of four distinct units and their corresponding percentage of unconsolidated material by thickness as: 52.6% clay/silt, 20.1% till, 20.9% sand, and 3.1% gravel, with the remaining 3.3% unknown due to lack of description in the WCRs. Percents were calculated by the following equation: (Σ sediment type thickness) / (Σ unconsolidated sediment thickness). Analyzed WCR data was then displayed in 3-D using Rockworks to get a general picture of the subsurface geology. Additionally, four geophysical methods: seismic, radar, time-domain electromagnetics, and electrical resistivity imaging (ERI), were tested at the RS-18 site along a 200m transect. ERI was the only tested method that successfully identified the sand body in this geologic setting.

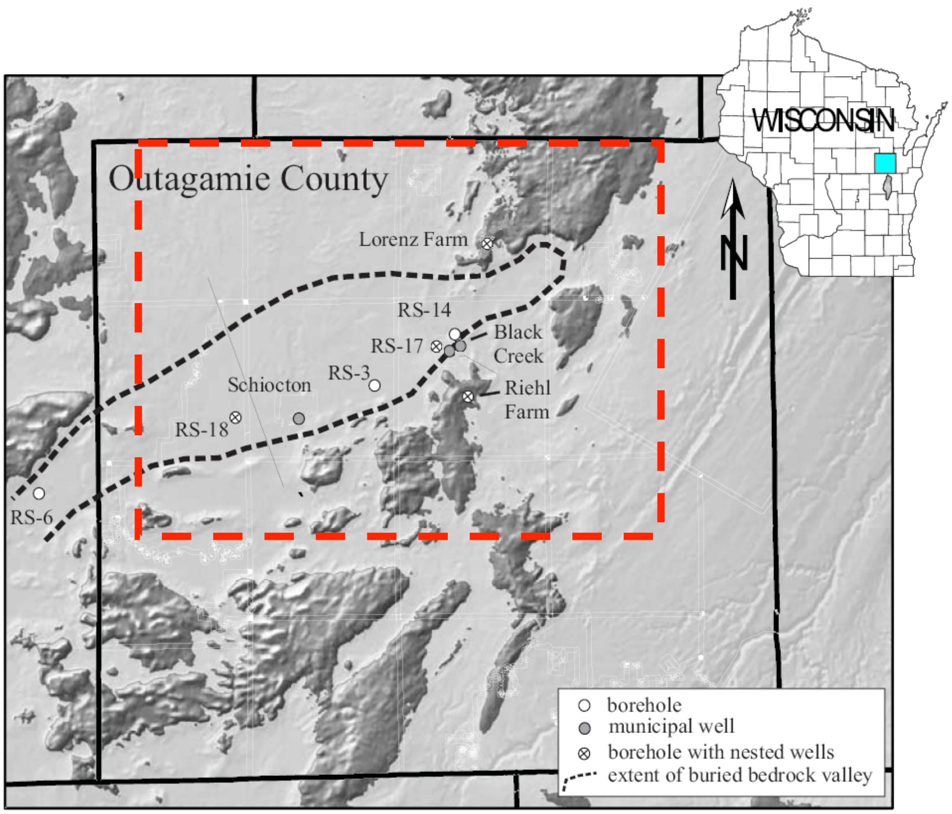

Figure 1. Shaded relief map of Outagamie County showing the lateral margins of the buried bedrock valley and locations of boreholes and wells drilled by the WGNHS. The dashed red box indicates the approximate location of the hydrostratigraphic and groundwater flow models. The light gray regions approximate the area covered by glacial Lake Oshkosh during the last glaciation. The inset shows the location of Outagamie County in WI. (modified from Hooyer *et al.*, 2008)

As part of this project, ERI was used at an additional eight sites, with geoprobe sampling at two of the sites confirming the geophysical interpretations. Then multiple-point geostatistics (Guardino & Srivastava, 1993) was used to create 300 three-dimensional hydrostratigraphic models for the representative site in Outagamie County, Wisconsin (Fig. 1), using as input data a combination of WCRs, electrical resistivity imaging, geoprobe sampling, and reasonable depositional histories determined from WCRs and five known outlets of glacial Lake Oshkosh . Multiple-point geostatistics uses training images, either 2-D or 3-D, that represent the general features of the subsurface (i.e., channels, lenses).

Training images have advantages over variograms, the more traditional geostatistical approach, because training images can include soft data, such as outcrops or geophysics, and can maintain geologic structure and continuity. All 300 hydrostratigraphic models were analyzed for statistics of connectivity using CONNEC3D (Pardo-Igúzquiza & Dowd, 2003) and a representative set of six hydrostratigraphic models was selected and imported into groundwater flow and transport models based on these analyses. The United States Geological Survey's (USGS) Modular Ground-Water Flow Model, MODFLOW-2000 (Harbaugh *et al*., 2000), was used to simulate groundwater flow in the six selected hydrostratigraphic models. The groundwater flow models were calibrated to head data, the calibration was checked with streamflow measurements, and particle tracking was performed and compared to statistics of connectivity. In addition to delineating preferential flow paths in a glacially-deposited aquitard, objectives included demonstrating the use of multiple-point geostatistics, understanding the flow system in Outagamie County, and reviewing and revising the depositional history of glacial Lake Oshkosh.

PROCEDURES AND METHODS

The hydrostratigraphic models incorporated hard and soft data to represent the possible range of deposits in the subsurface. Hard data are generally geologic or hydrogeologic data at point locations, such as boring logs or hydraulic conductivity measurements, while soft data are generally non-point data and include geophysical logs, outcrop information, or knowledge of the depositional environment. Additionally, these data were used to interpret the provenance of the sand bodies. While glacial in origin, their provenance is unknown. They could be beach deposits, underflow/subaqueous fan type deposits, or perhaps both are present in different areas of the lacustrine sediments.

As described above, ERI was used at an additional 8 sites, with analysis of the imaging used to determine the average and range of sizes of the sand bodies. Several of the sites had more than one ERI transect performed, for a total of 14 ERI transects (See Appendix B and Fig. 2). Every transect had higher resistivity values at depth and three of the transects also had higher values at the surface, indicating the presence of sand (Fig. 2). Hand augering to a depth of 5 ft at both sites with higher surface resistivity values confirmed the presence of sand. The three transects with sand at the surface also had higher resistivity values than the other transects, indicating sand at these sites may be coarser. All of the ERI was done with 5 m (16.4 ft) spacing and a Wenner alpha array, and all transects were 115 m (~377 ft) in length, except for RS-18 transect 1b, which was 195 m (~640 ft). The inversions were performed with the RES2DINV software (Geotomo Software, Malaysia), using a standard Gauss-Newton inversion. The following parameters were used for the inversion process: initial damping factor of 0.160, minimum damping factor of 0.015, relative changes in root mean square (RMS) error for convergence of 5, minimum change in RMS error for line search of 0.4, and the maximum number of iterations was 20. Geoprobe sampling at two sites confirmed the geophysical interpretations, including coarser sand present at sites with higher resistivity values. See Appendix C for the core logs.

Present day elevations of 1,629 sand and gravel bodies were determined from WCR location data and digital elevation models (DEMs), with the use of ArcGIS software. Then using results from the Clark model (Clark et al., 2007; Clark et al., 2008) to account for rebound, the elevations of the sand and gravel bodies were compared to the five known outlets of glacial Lake Oshkosh (Fig. 3). The Clark model uses predictions of glacial isostasy and digital elevation data to determine the paleo-topography, and to create a paleo DEM. Extensions of the ArcGIS and GRASS (Geographic Resources Analysis Support System) software that determine drainage basins from DEMs were used to define the lake size and outlet. It is important to note that the predicted shorelines determined by the Clark model represent a minimum lake extent. Therefore, if the sand body elevations match up with those of the outlets or are higher than the outlet, this would indicate that the sand bodies are most likely beach deposits. If the sand body elevations are lower than the outlets, then the sand bodies are likely underflow deposits, although it should be noted that much lower sand bodies could be beach deposits from an earlier lake level. Analysis of the high K

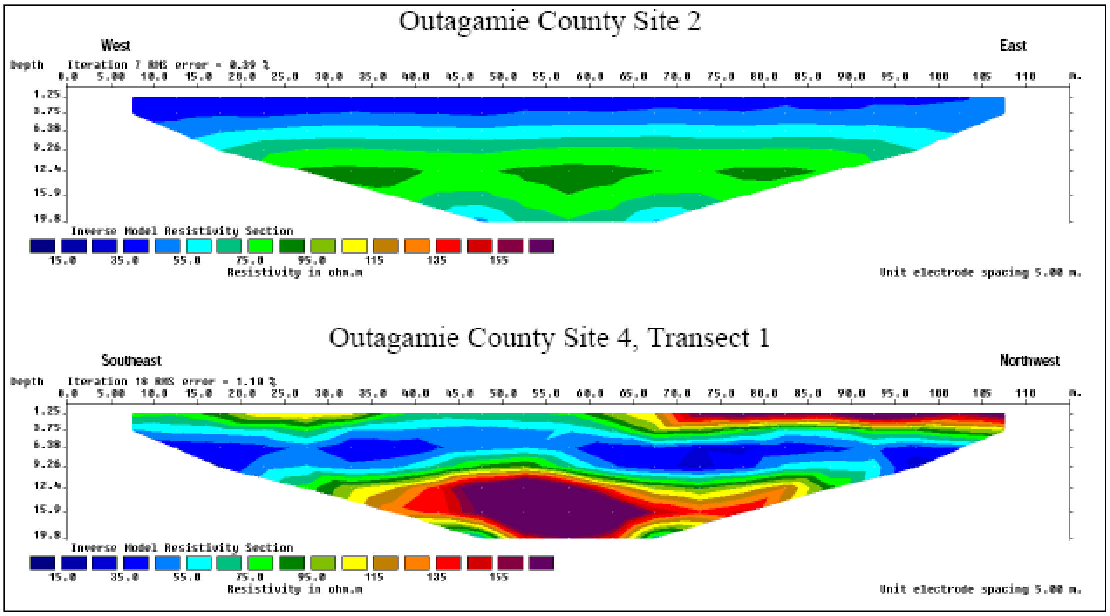

Figure 2. Electrical Resistivity Image for two of the additional sites: OU-2, located in the central western portion of the buried bedrock valley and OU-4, located in the northern central portion of the buried bedrock valley. Note the higher resistivity units at the surface at OU-4 and at depth at both sites, most likely sand. At OU-4 hand augering to a depth of 5 ft (1.5 m) confirmed sand in the near surface and geoprobe sampling to a depth of 55 ft (16.8 m) confirmed sand at depth. Units are in meters and ohm-meters.

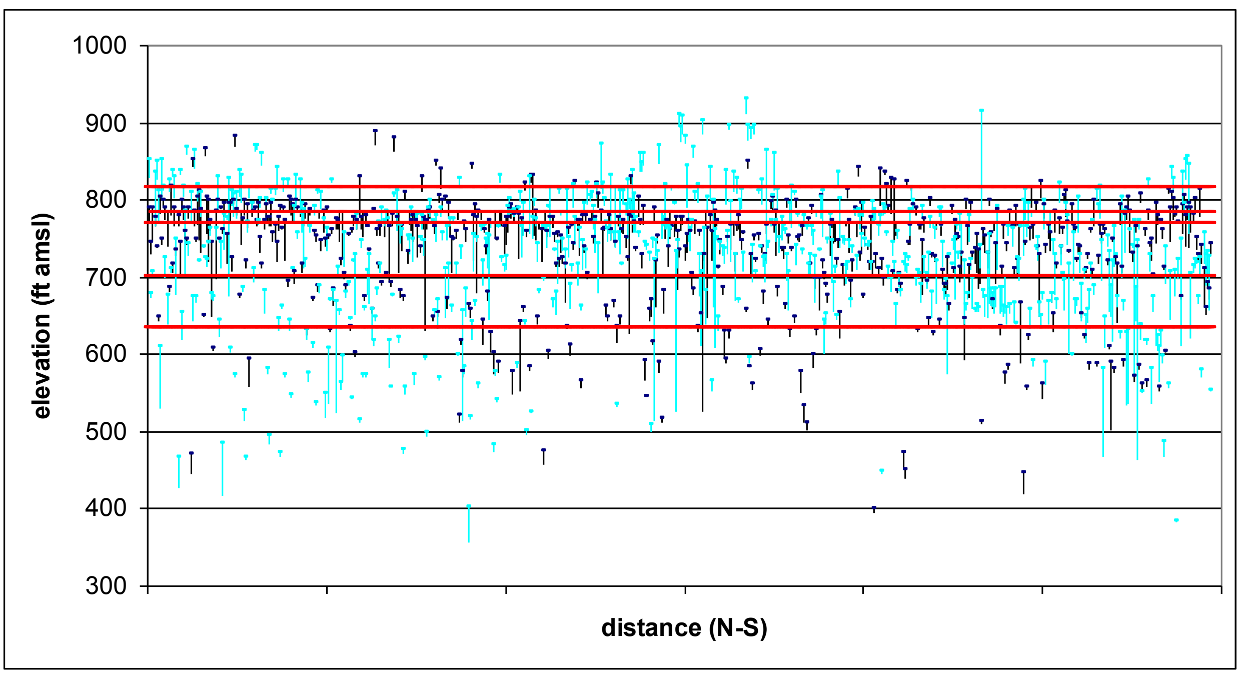

Figure 3. Comparison of the elevations of the sand (dark blue) and gravel (light blue) bodies to the elevations of the five known lake outlets (red). Note that the majority of the deposits below the lowest lake elevation are gravel, indicating underflow type deposits.

deposits (sand and gravel) indicates 10% of the total number of deposits are above the highest lake level (785 ft), while 26% are below the lowest lake level (636 ft). The majority of the deposits are less than 30 ft above the highest lake level, but a few may be dune deposits as they are nearly 100 ft above the highest lake level. Overall, these analyses indicated the deposits are likely a combination of beach and underflow deposits. Additionally, the 3-D display of WCRs (Fig. 4) indicates there may be slightly more gravel to the east and deeper than the sand bodies, which suggests underflow or subqueous fan type deposits.

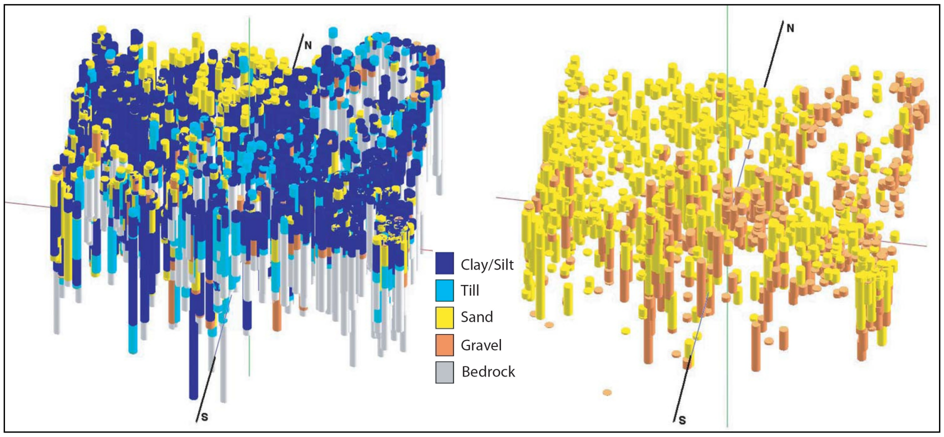

Figure 4. WCRs displayed in 3-D for the area shown in Fig. 1 (dashed red box). All units displayed on left, high K units only displayed on right (created in Rockworks, 2006).

The hard and soft data were used to create 300 hydrostratigraphic models using the Stanford Geostatistical Modeling Software (SGeMS) (Remy et al., 2009), which has the algorithm for multiple-point geostatistics and has a training image generator (TIGENERATOR). Multiple-point geostatistics, which was first suggested to model subsurface heterogeneity by Guardiano and Srivastava (1993), but not used much until the single normal equation simulation (snesim) algorithm was developed by Strebelle (2000, 2002), reducing the computation time. Multiple-point geostatistics uses one or more training images, which can be either 2-D or 3-D, to represent the general features of the subsurface (i.e., channels, lenses), rather than a variogram. Each node is then simulated by conditional probabilities based on the probability of occurrences of data events (patterns of a defined size) within the training image, hard data (if available), and previously simulated nodes. Thus, the training image must be scanned for each node, a computationally intensive procedure. The snesim algorithm reduces computation time by scanning the training image only once and saving the distributions of patterns in a search tree. Details of multiple-point geostatistics and the snesim algorithm can be found in the above cited papers as well as a review paper by Hu and Chugunova (2008). To create the 300 hydrostratigraphic models several steps had to be performed. First, a model grid was defined. Then 80 training images were created, with a subset of these selected for use in the snesim algorithm based on visual comparison with the 3-D WCR display (Fig. 4) and general geologic plausibility. Finally, hard data were imported and parameters were defined and analyzed during the running of the snesim algorithm. Details of the process are described in Appendix D.

All 300 hydrostratigraphic models were analyzed for connectivity statistics using CONNEC3D (Pardo-Igúzquiza & Dowd, 2003), which calculates a number of connectivity statistics and writes these to several output files (see Appendix E for more details). Statistics from all 300 models were imported into an Excel file and analyzed. Of the 300 models, 240 have statistically and geologically acceptable parameters (see Appendix D for more details) and were considered in the selection process for a representative set of models that were imported into groundwater flow models. Selection of the six representative models was based on analyses of the connectivity statistics, especially three connectivity statistics with more variability than the others. Details of the model selection are in Appendix F.

The USGS Modular Ground-Water Flow Model, MODFLOW-2000 (Harbaugh *et al*., 2000), was used to simulate groundwater flow in the six selected hydrostratigraphic models. This code was chosen because of its capabilities to simulate three-dimensional groundwater flow in steady-state and incorporate the hydrostratigraphic model data. The pre- and post-processor Groundwater Vistas (GWV) Version 6.15 (Rumbaugh & Rumbaugh, 2012) was used to set up and run the models. The code PEST (Doherty, 2004), which is a parameter estimation routine, was used to calibrate the models. The modular three-dimensional multispecies transport model, MT3DMS, (Zheng & Wang, 1999) was used to model $\delta^{18}O$ movement in the calibrated groundwater flow models to determine if the anomalous recent water found at depth (Hooyer *et* al., 2008) could be explained by preferential flow paths. The particle tracking code MODPATH (Pollock, 1994) was used to determine groundwater flow pathways through the glacial Lake Oshkosh sediments, particularly in the deepest parts of the buried bedrock valley. The MODFLOW models were solved using the PCG2 solver (Hill, 1990), which uses both head change and mass-balance as convergence criteria. Details of the groundwater flow and transport models are in Appendix G.

RESULTS AND DISCUSSION

Connectivity statistics had one or more percolating paths (a single connected component that connects from one end to the other in a specific direction) in the z-direction for every hydrostratigraphic model, indicating preferential flow is likely occurring vertically through the glacial sediments. Particle tracking results confirmed this. One particle was placed at the top of each cell in the approximate horizontal extent of the bedrock valley of layer 2 and tracked forward in time, for a total of 2,108 particles. Every model had particles exit in the deeper regions of the bedrock valley (layers 60-83). Also, every model had 42-58% of the total particles exit in the first layer. The percent of particles to exit the constant head boundary in layers 40-83 after traveling at least halfway through the valley vertically varied from 10-18%. Only a small percent (0.33-1.66%) of particles moved vertically into the deepest portions of the bedrock valley (layer 60-83) before exiting (Fig. 5). There also was vertical movement in shallower areas of the valley, often through clay (Fig. 6).

Particles were also placed in every non-boundary cell at the top of layer 2 of the model and tracked forward in time. Results were analyzed for total travel time to a bedrock head boundary. In order to do this, all particles exiting the model at a non-bedrock boundary were removed from the analysis. Among all six models, a total of 25,906 particles traveled through the glacial sediment in the bedrock valley and exited into the bedrock. Results confirmed that flow is largely vertical, with a maximum horizontal particle movement of 11 cells and only 5.2% of the total particles moving horizontally. Results indicated that preferential flow may be occurring, as 6.77% of the particles take fewer than 100 years to move to the bedrock. Percents for eight different time periods are displayed in Figure 7. Since the majority of the particles take between 100 and 10,000 years to move through the model, the small percent moving faster may be indicative of preferential flow. Previous isotope measurements, in particular $\delta^{18}O$, found anomalous recent water at depth (Hooyer *et al*., 2008). Preferential flow paths could explain these measurements, but with the majority of particles moving through the valley in fewer than 10,000 years, glacial age water would be largely flushed out of the valley deposits. However, approximately 28% of the simulated isotope values from the MT3DMS simulations (Appendix G) are glacial age values. This discrepancy is likely due to the majority of the particles either moving through the shallower regions of the bedrock valley or through preferential flow paths in the deeper regions of the bedrock valley. There could be additional factors contributing to the overall particle travel times being too fast for glacial age water to remain in the lacustrine deposits, including: the lateral and bottom boundary conditions, lack of understanding recharge in the system, cell size too large, clay K too high, or perhaps there should be more preferential pathways with less overall vertical flow in the clay matrix.

Additional evidence for preferential flow was provided by running a model with a uniform value of K equal to the volumetrically weighted mean K and analyzing travel times for particles placed in every non-boundary cell of layer 2. Compared to the statistics for the six hydrostratigraphic models, travel times are much more uniform, with 90% of particles taking 100-1,000 years. Visual analysis of particles confirms all particles are moving at the same rate.

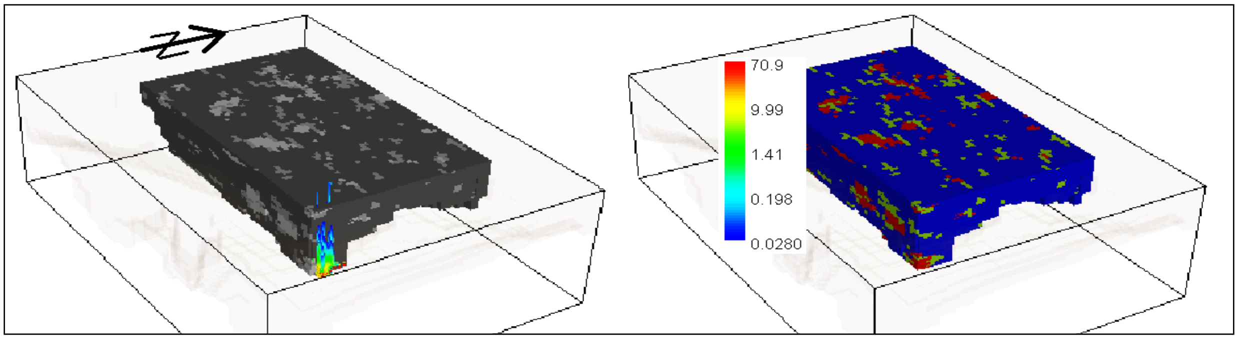

Figure 5. Examples of particle tracking shown as pathways in deeper areas of the bedrock valley for model 10_7. The particles are shown on the left, with blue indicating earlier times, yellow and red later. All particles shown moved through the valley in 1,000 years or less. North is indicated on the particle diagram. The same region is shown on the right, with K values (ft/d) indicating the fine-grained glacial are blue, with coarser deposits yellow and red. 50x vertical exaggeration.

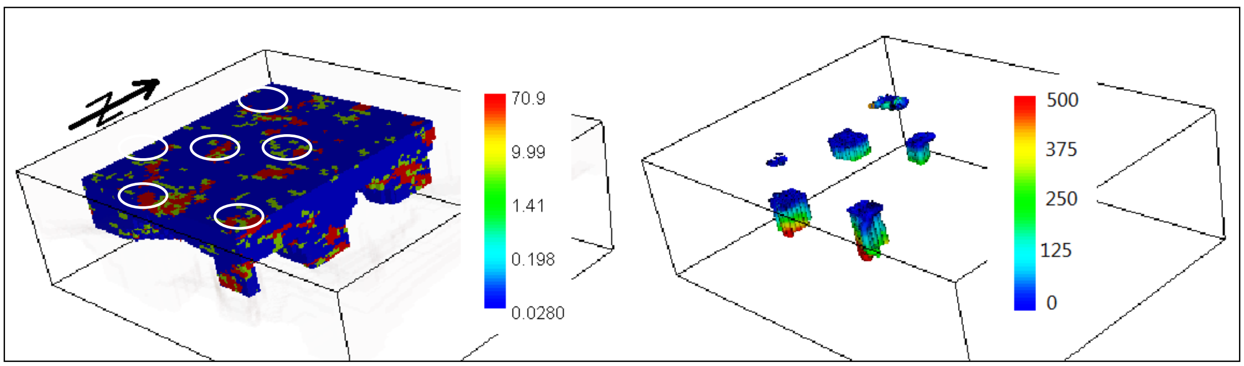

Figure 6 Examples of particle tracking shown as pathways in shallower areas of the bedrock valley for model 10_7. On the left, K values (ft/d) indicate the fine-grained glacial deposits are blue, with coarser deposits yellow and red. On the right, particles tracks are displayed by time in years. North is indicated on the K value image. White ovals on the K figure indicate approximate locations of particle clusters. Note that comparing these two indicates the higher K units are allowing faster movement of particles. 50x vertical exaggeration.

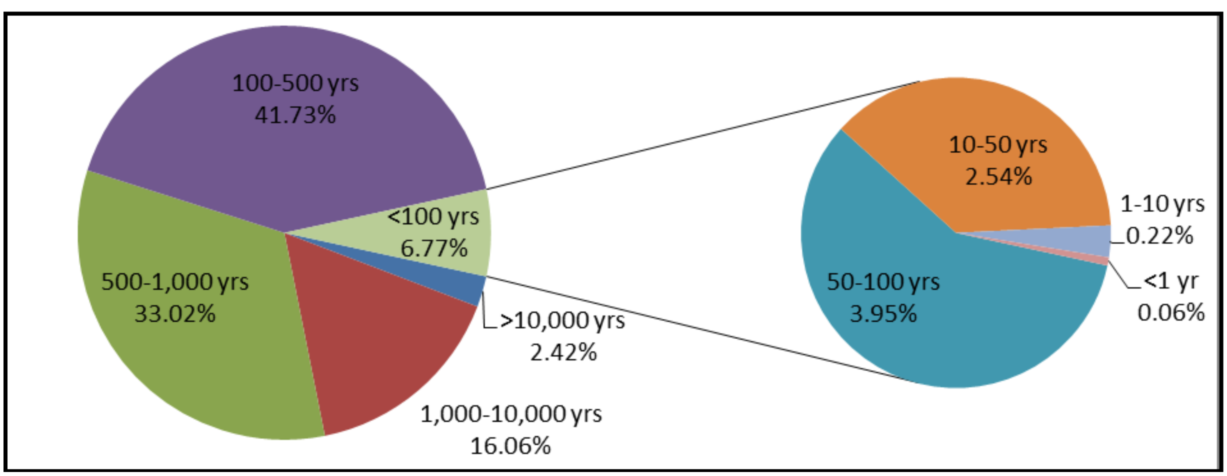

Figure 7. Pie chart of percent of particles taking a given length of time to move through the glacial sediments and into the surrounding bedrock. The chart on the right breaks down the travel times for particles taking fewer than 100 years. Results are combined for all six models.

In addition to the particle travel times and isotope evidence for preferential flow, individual flow paths can be traced vertically through the valley in all six models (Table 1). As an example, in model 10_7 two particles, 62 and 94 are 1.3 miles apart in layer 2 and both exit into the bedrock in layer 44. However, particle 62 takes 3,425 years, while particle 94 takes only 96 years. Examination of the hydrostratigraphy indicates that particle 62 moves vertically through clay 3,311 of these years, before finding a high K unit and eventually exiting the valley, while particle 94 is in a high K unit for most of its pathway.

Table 1. Examples of preferential flow through comparison of individual particles. Starting and ending separation is the distance between particles at their starting and ending locations. All particles start in layer 2. Lithology is described in percent by cells traveled through, with only the dominant lithology listed as a percent.

Model	Particle #	Starting Separation (mi)	Exiting Layer	Ending Separation (mi)	Travel Time (yrs)	Lithology
10_7	94	1.3	44	0	96	92.9 % sand/gravel (clay at surface)
10_7	62				3,425	97.6% clay (gravel at depth)
18_7	3153	2.9	82	2.4	2,487	61.9% clay (sand interspersing)
18_7	3454				32,247	100% clay
18_7	5753	1.3	33	0.3	4	100% sand
18_7	6049				2,129	56.3% clay (sand at depth)
19_8	2509	0.5	23	0.5	62	100% sand
19_8	2510				235	81.8% sand (clay at surface)
19_8	2511				500	100% clay
22_6	5173	1.2	29	1.1	46	92.9% sand/gravel (clay at depth)
22_6	4686				1,627	92.9% clay (sand at surface)
25_9	4243	0.9	33	0.9	10	100% sand/gravel
25_9	4630				1,036	100% clay
29_4	190	0.45	19	0.45	3	64.7% sand/gravel (clay interspersing)
29_4	188				232	100% clay

CONCLUSIONS AND RECOMMENDATIONS

This is one of the first examples demonstrating the application of multiple-point geostatistics in three-dimensions to a field site using a variety of field data, including geophysics. Previous work either used synthetic data (Feyen & Caers, 2005; Liu, 2006; Michael *et al*., 2010), was used in mining applications and incorporated traditional geostatistics into the training images (Bastante *et al.*, 2008), was used to model at the pore scale (Lu *et al*, 2009), only modeled in two-dimensions (Huysmans & Dassargues, 2009), or focused on combining multiple-point simulations with other types of data and models (Michael *et al*., 2010).

Preferential flow is likely occurring in glacial Lake Oshkosh sediment as indicated by the analysis of the connectivity statistics for the hydrostratigraphic models and results of the particle tracking. All 300 hydrostratigraphic models had one or more percolating components in the z-direction. Also, the particle tracking indicated that for all six groundwater flow models, over 6% of the particles were moving through the bedrock valley in fewer than 100 years; examples of particles moving faster through high K units were found in each model. Additionally, this work demonstrates that preferential flow can occur in a glacially-deposited aquitard through connected sand bodies without the presence of fractures, and is likely occurring in similar types of deposits, especially those that are more fractured, such as clayey tills. Overall, results of the statistics of connectivity and particle tracking indicate that a hydrostratigraphic model with fewer, longer pathways or one with many shorter pathways can create preferential flow paths and can calibrate to head and streamflow data. Additionally, the origin of the sand and gravel deposits is most likely a combination of beach and underflow deposits as demonstrated by the WCR data.

Based on the calibrations to the head targets and check on the calibration with the stream fluxes, the six models are all equally likely representations of the sediments. However, the groundwater flow models should be better calibrated in order to use them for purposes of groundwater management in Outagamie County. This will require a joint calibration of groundwater flow and transport models (with oxygen isotope data) as well as collection of additional head, stream flux, and isotope targets.

REFERENCES

Bastante, F.G., Ordóñez, C., Taboada, J., and Matias, J.M., 2008. Comparison of indicator kriging, conditional indicator simulation and multiple-point statistics used to model slate deposits. *Engineering Geology*, vol. 98, p. 50-59.

Cherry, J.A., Parker, B.L., Bradbury, K.R., Eaton, T.T., Gotkowitz, M.G., Hart, D.J., and Borchardt, M. 2006. Contaminant Transport through Aquitards: A State-of-the-Science Review. Denver, Colorado: American Water Works Association Research Foundation.

Clark, James A., Zylstra, Deborah J., and Befus, Kevin M., 2007. Effects of Great Lakes Water Loading upon Glacial Isostatic Adjustment and Lake History. *Journal of Great Lakes Resources*, vol. 33. p. 627-641.

Clark, James A., Befus, Kevin M., Hooyer, Thomas S., Stewart, Peter W., Shipman, Taylor D., Gregory, Chris T., and Zylstra, Deborah J., 2008. Numerical simulation of the paleohydrology of glacial Lake Oshkosh, eastern Wisconsin, USA. *Quaternary Research*, vol. 69, p. 117-129.

Doherty, J. 2004. PEST, Model-Independent Parameter Estimation: Watermark Numerical Computing.

Feyen, L. and Caers, J., 2005. Multiple-point geostatistics; a powerful tool to improve groundwater flow and transport predictions in multi-modal formations. Proceedings-European Conference on Geostatistics for Environmental Applications, vol. 5, p. 197-207.

Gerber, Richard E., Boyce, Joseph I., and Howard, Ken W.F. 2001. Evaluation of heterogeneity and field-scale groundwater flow regime in a leaky till aquitard. *Hydrogeology Journal*. Vol. 9, p. 60-78.

Grisak, G.E. and Cherry, J.A., 1975. Hydrologic characteristics and response of fractured till and clay confining a shallow aquifer. *Canadian Geotechnical Journal*, vol. 12, p. 23-43.

Guardiano, F. and Srivastava, M. 1993. Multivariate geostatistics: Beyond bivariate moments, in *Geostatistics Troia'92*, ed. A. Soares. P. 133-144.

Harbaugh, A.W., Banta, E.R., Hill, M.C., and McDonald, M.G. 2000. MODFLOW-2000, The U.S. Geological Survey modular ground-water model- user guide to modularization concepts and the ground-water flow process. U.S. Geological Survey Open-File Report 00-92.

Hill, M.C. 1990. Preconditioned Conjugate-Gradient 2, A Computer Program for Solving Ground-Water Flow Equations: U.S. Geological Survey, Water-Resources Investigations Report 90-4048.

Hooyer, T.S., Hart, D.J., Bradbury, K.R., and Batten, W.G., 2008. Investigating groundwater recharge to the Cambrian-Ordovician Aquifer through fine-grained glacial deposits in the Fox River Valley: Final Report to the Wisconsin Department of Natural Resources.

Hu, L.Y. and Chugunova, T., 2008. Multiple-point geostatistics for modeling subsurface heterogeneity: A comprehensive review. *Water Resources Research*, vol. 44, W11413.

Huysmans, Marijke and Dassargues, Alain, 2009. Application of multiple-point geostatistics on modelling groundwater flow and transport in a cross-bedded aquifer (Belgium). *Hydrogeology Journal*, vol. 17, p. 1901-1911.

Liu, Yuhong, 2006. Using the *Snesim* program for multiple-point statistical simulation. *Computers & Geosciences*, vol. 32, p. 1544-1563.

Lu, DeTang, Zhang, Ting, Yang, JiaQing, Li, DaoLun, and Kong, XiangYan, 2009. An Improved Reconstruction Method for Porous Media Based on Multiple-point Geostatistics. *Chinese Science* Bulletion, vol. 54, no.11, p 1876-1885.

Michael, H.A., Li, H., Boucher, A., Sun, T., Caers, J., and Gorelick, S.M., 2010. Combining geologic-process models and geostatistics for conditional simulation of 3-D surface heterogeneity. *Water Resources Research*, vol. 46, W05527, 20 pages.

Pardo-Igúzquiza, Eulogio and Dowd, Peter A., 2003. CONNEC3D: a computer program for connectivity analysis of 3D random set models. *Computers and Geosciences*, vol. 29, p. 775-785.

Perry, E.C. Jr., Grundl, T., and Gilkeson, R.H., 1982. H, O, and S isotopic study of the groundwater in the Cambrian-Ordovician aquifer system of northern Illinois. In: Perry, E.C. Jr. and Montgomery, C.W., Eds. Isotopic Studies of Hydrologic Processes. Northern Illinois Univ. Press, p. 35-43.

Pollock, D.W. 1994. User's Guide for MODPATH/MODPATH-PLOT, Version 3: A particle tracking post-processing package for MODFLOW, the U.S. Geological Survey finite-difference ground-water flow model: U.S. Geological Survey, Open-File Report 94-464.

Remy, Nicolas, Boucher, Alexandre, and Wu, Jianbing, 2009. Applied geostatistics with SGeMS; a user's guide, Cambridge University Press, New York, 110 p.

Rumbaugh, J. O., and Rumbaugh, D. B. 2007. Groundwater Vistas, version 5. Environmental Solutions Inc., Reinholds, PA, www.groundwatermodels.com.

Siegel, D.I. and Mandle, R.J., 1984. Isotopic Evidence for Glacial Meltwater Recharge to the Cambrian-Ordovician Aquifer, North-Central United States. *Quaternary Research*, vol. 22, p. 328-335.

Strebelle, 2000. Sequential simulation drawing structures from training images: Ph.D. diss., Stanford.

Strebelle, 2002. Conditional simulation of complex geological structures using multiple-point statistics. *Mathematical Geology*, vol. 34, no. 1, p 1-21.

Zheng, Chunmiao and Wang, P. Patrick, 1999. MT3DMS: A Modular Three-Dimensional Multispecies Transport Model for Simulation of Advection, Dispersion, and Chemical Reactions of Contaminants in Groundwater Systems; Documentation and User's Guide; U.S. Army Engineer Research and Development Center Contract Report SERDP-99-1, Vicksburg, Mississippi, 202 p.

APPENDIX A: Awards, Presentations, Reports, Patents and Presentations

1) Dunkle, K.M., Hart, D.J., and Anderson, M.P., 2013. Groundwater flow model calibration difficulties in areas with glacially-deposited aquitards: An example from glacial Lake Oshkosh, Geological Society of America *Abstracts with Programs*, vol. 45, no. 4, p. 53.
   Presented: May 3, 2013 in Kalamazoo, Michigan

2) Dunkle, K.M., Hart, D.J., and Anderson, M.P., 2012. Preferential flow paths in glacial Lake Oshkosh sediment, Outagamie County, WI, Geological Society of America *Abstracts with Programs*, vol. 44, no. 7, p. 145.
   Presented: November 4, 2012 in Charlotte, North Carolina

3) Dunkle, K.M., Hart, D.J., and Anderson, M.P., 2011. Hydrostratigraphic & groundwater flow models for glacial Lake Oshkosh sediment, Outagamie County, WI, Geological Society of America *Abstracts with Programs*, vol. 43, no. 5, p.560.
   Presented: October 12, 2011 in Minneapolis, Minnesota

4) Dunkle, K.M., Hart, D.J., and Anderson, M.P., 2011. Multiple-point geostatistics for creation of 3D hydrostratigraphic models, Outagamie County, WI, Three Dimensional Geological Mapping: Workshop Extended Abstracts, Geological Survey of Canada, Open File 6998.
   Presented: October 8, 2011in Minneapolis, Minnesota

APPENDIX B: Electrical Resistivity Imaging

Location of Electrical Resistivity Imaging sites in modeling area (Fig. 1: dashed red box). Dashed line is approximate extent of pre-glacial buried bedrock valley. Pale green lines outline the townships, which are 6 x 6 miles.

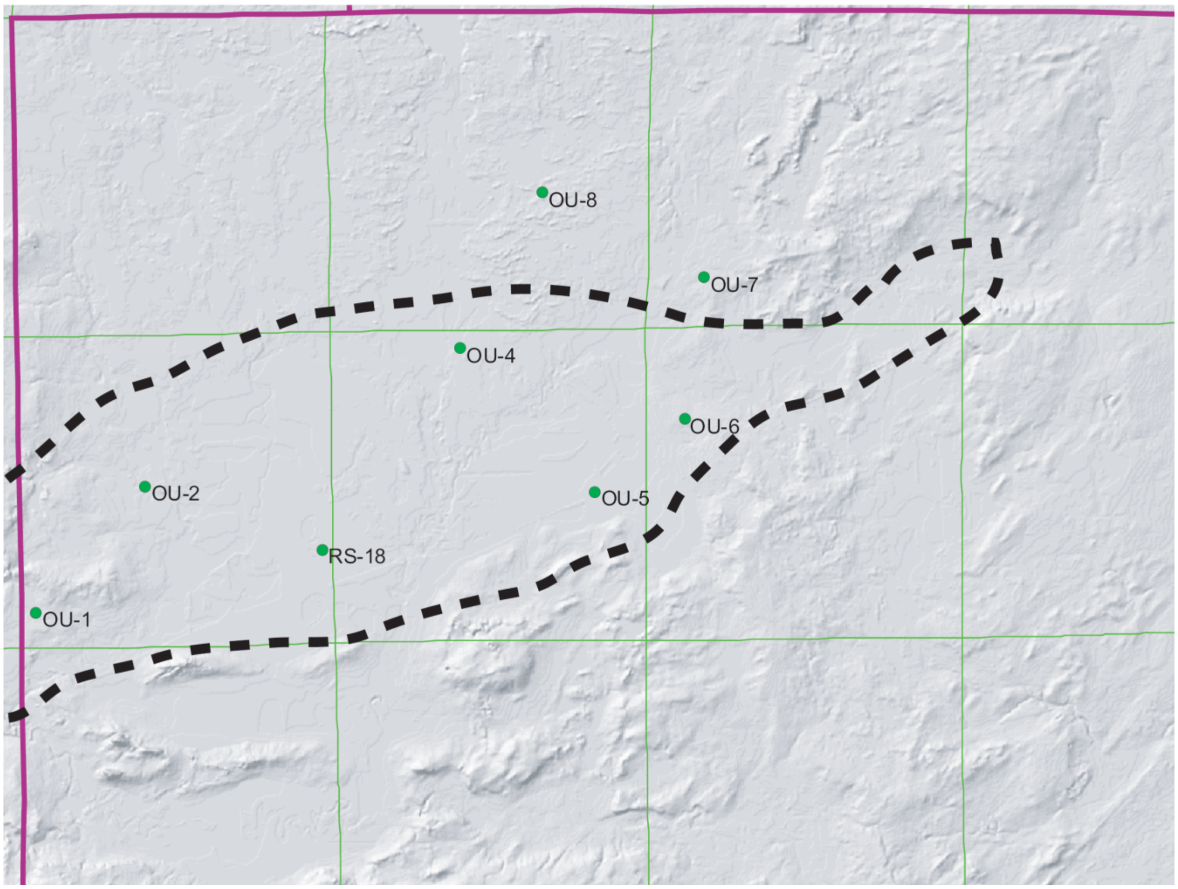

.

RS-18, Transect 1a*

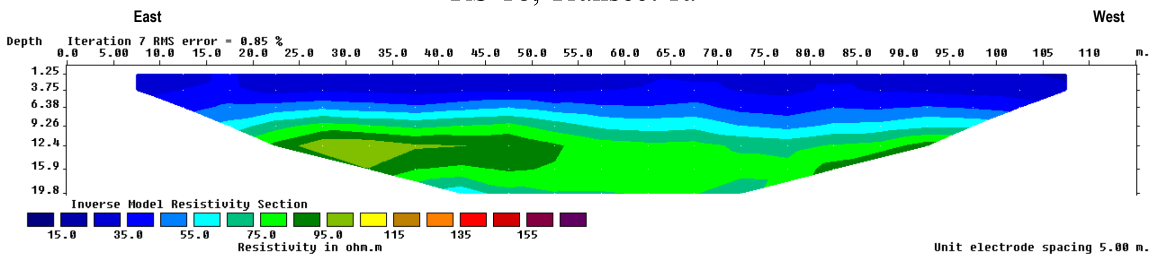

RS-18, Transect 1b*

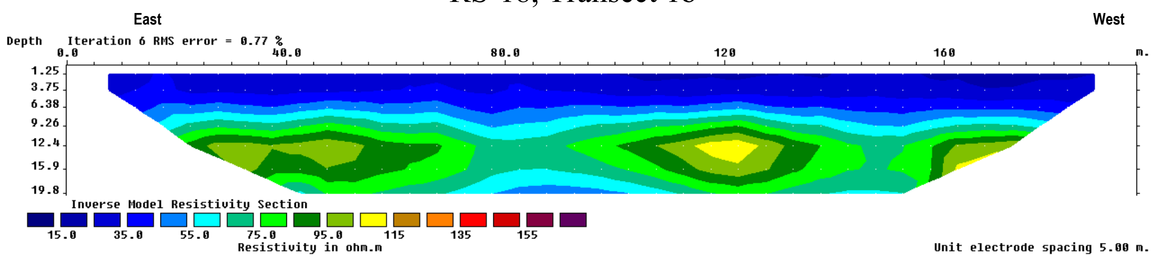

RS-18, Transect 2

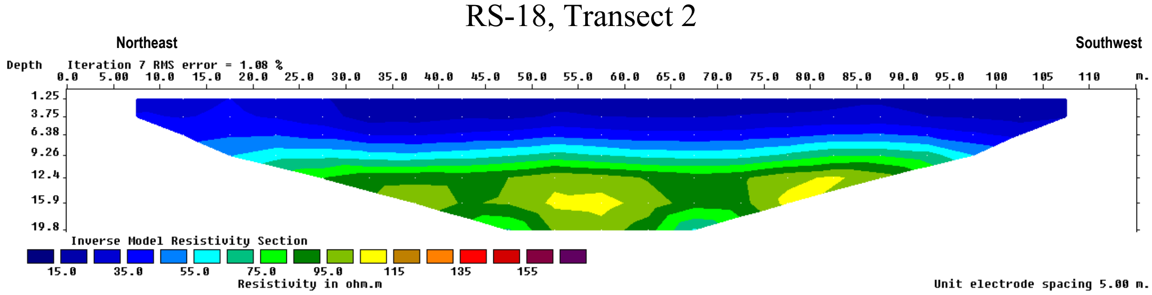

*Note that transects 1a and 1b have the same starting location and direction.

Outagamie County Site 1, Transect 1

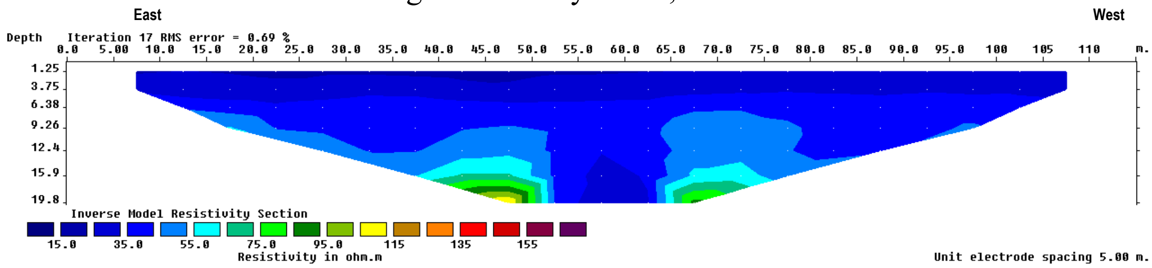

Outagamie County Site 1, Transect 2

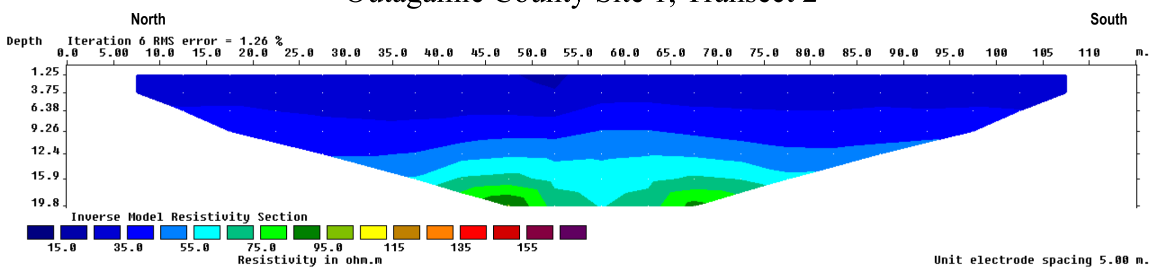

Outagamie County Site 6, Transect 1

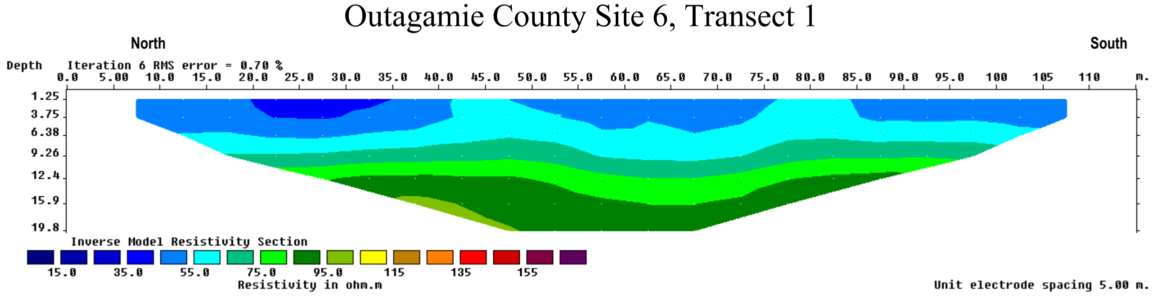

Outagamie County Site 6, Transect 2

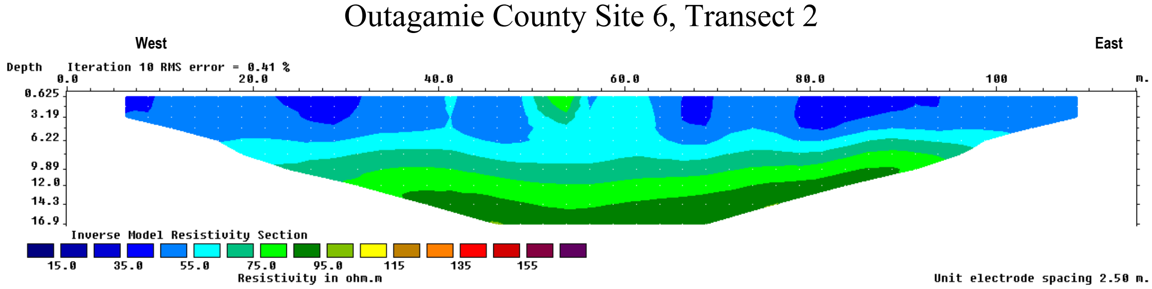

Outagamie County Site 7, Transect 1

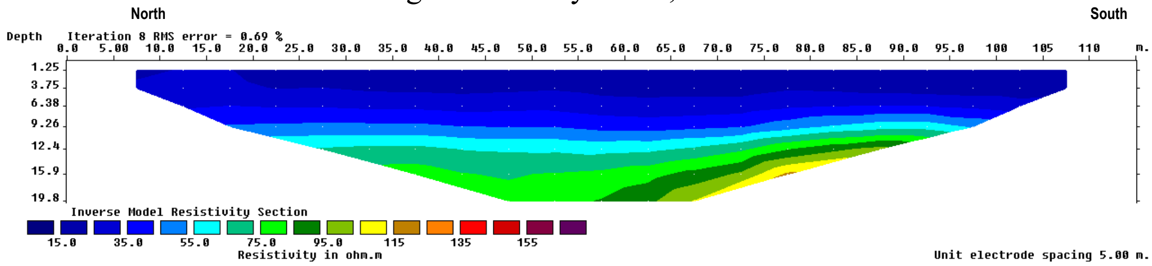

Outagamie County Site 7, Transect 2

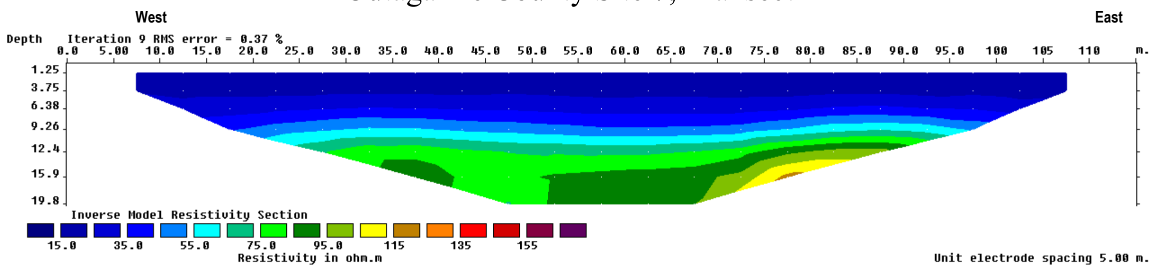

Outagamie County Site 4, Transect 1

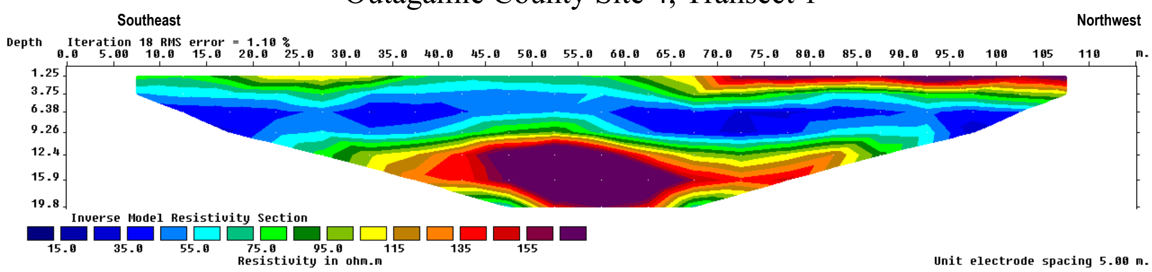

Outagamie County Site 4, Transect 2

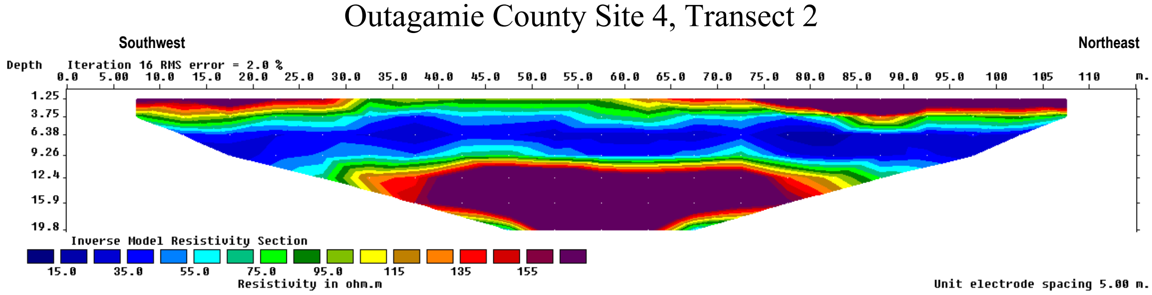

Outagamie County Site 2**

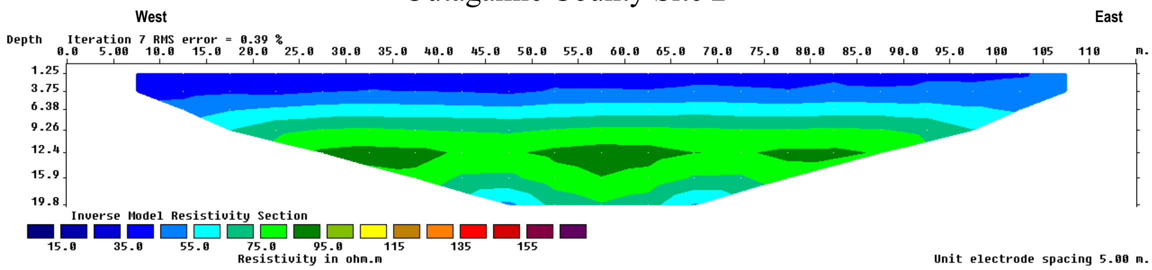

Outagamie County Site 5**

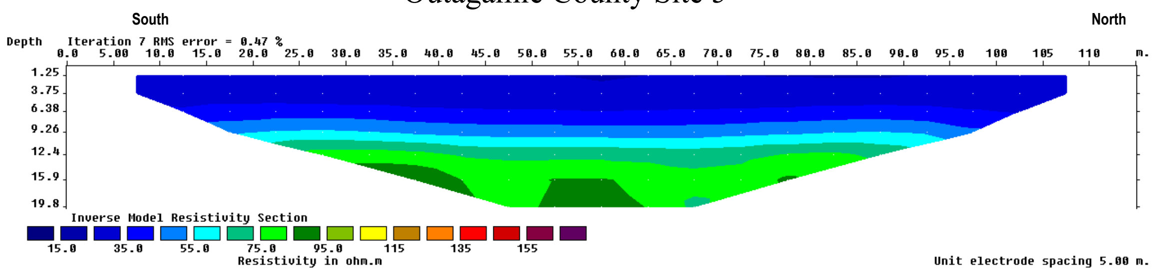

Outagamie County Site 8**

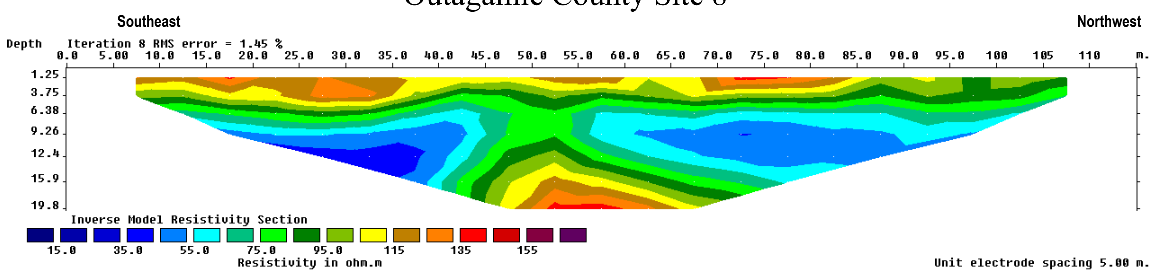

**Only one transect done at each of these sites due to various field settings:
OU-2: road and railroad at this location
OU-5: stream running through the property
OU-8: frozen/partially frozen ponds through woods; note hand augering confirmed sand in the near surface

APPENDIX C: Geoprobe Logs

Note sampling done in 5 ft increments for all cores.

RS-18 Core #1

Depth (ft)	Description
0-5	***40% recovery, all at bottom of sleeve***
3-3.3	Gasket
3.3-3.6	Very fine sand, dark matter (organics?), abrupt contact at 3.6 ft
3.6-5	Fine to very fine sand, well to very well rounded, laminations (dark); from 4.05-4.3 ft, soft, little clayey
5-10	***100% recovery, lots of water in the bottom***
5-6	Fine to very fine sand with dark spots
6-7.5	Fine to very fine sand
7.5-8.2	Transition
8.2-10	Clay with fine sand; sticky clay layer from 9.25-9.35 ft
10-15	***100% recovery***
10-12.7	Clay with fine sand
12.7-15	Clay, sticky; few black organics at end (possibly sluff)
15-20	***96% recovery, missing bottom***
15-15.9	Clay with fine sand (less sand than above)
15.9-19.8	Clay, sticky
20-25	***100% recovery***
20-21.05	Clay with fine sand; abrupt contact at 21.05 ft
21.05-25	Clay, sticky
25-30	***100% recovery***
25-26.05	Clay with varves; few dark spots 25.45-25.9 ft (organics or mineral core?)
26.05-28.7	Clay with lower fine to very fine sand; harder than sticky clay
28.7-30	Clay, sticky
30-35	***100% recovery***
30-35	Clay, sticky with few varves
35-40	***100% recovery***
35-37.05	Clay, sticky, abrupt contact at 37.05
37.05-37.32	Upper fine to lower medium sand with organics; microscope examination indicated mostly quartz (~90%), with few dark fragments
37.32-40	Upper fine to lower medium sand; some patches upper medium
40-45	***92% recovery, bottom is sluff***
40-44.6	Upper fine to medium sand; lamination at 42.25 ft
45-50	***100% recovery***
45-48.05	Sandy-clay, coarsens downward from fine to upper fine; clay laminations/layers from 45.8-46.05 ft
48.05-50	Upper fine to lower medium sand

RS-18 Core #1-continued

Depth (ft)	Description
50-55	***100% recovery; maybe some sluff on top***
50-50.6	Upper fine to lower medium sand; abrupt contact at 50.6 ft; microscope examination indicated mostly quartz (~90%), with few dark fragments
50.6-51.2	Fine grained sandy discolorations
51.2-54.2	Sand clay/clayey sand; slowly coarsening upward
54.2-54.65	Clay (darker color) with sand (lighter color) laminations
54.65-55	Clay with fine sand

RS-18 Core #2

Depth (ft)	Description
0-30	***No sample taken…..geoprobe pushed through to only sample sand transition***
30-35	***88% recovery***
30.1-32.84	Clay, sticky; abrupt contact at 32.84 ft
32.84-34.32	Upper fine to lower medium sand (mostly lower)
34.32-35	Mostly missing, upper fine to lower medium sand on edges; microscope examination indicated mostly quartz (~90%), with few dark fragments
35-40	***100% recovery***
35-40	Upper fine to lower medium sand; few dark spots (organics/minerals); saturated; microscope examination indicated mostly quartz (~90%), with few dark fragments
40-45	***100% recovery***
40-41.11	Upper fine to medium sand; more fine than above
41.11-41.8	Upper fine to medium sand; more gray than brown; maybe some clay
41.8-43.1	Fine sand
43.1-43.4	Fine sand with clay; harder; orange in color
43.4-45	Fine sand
45-50	***100% recovery***
45-47.4	Fine sand; few dark spots; microscope examination indicated mostly quartz (~90%), with few dark fragments
47.4-48.6	Fine sandy clay
48.6-50	Fine sandy clay; more clay content then above; sticky clay interspersed

RS-18 Core #3

Depth (ft)	Description
0-30	***No sample taken…..geoprobe pushed through to only sample sand transition***
30-35	***96% recovery***
30.2-35	Clay, sticky
35-40	***100% recovery***
35-36.51	Clay, sticky; abrupt contact at 36.51 ft
36.51-36.78	Fine sand; very dark
36.78-38.4	Fine to lower medium sand with clay skins
38.4-40	Fine to lower medium sand; microscope examination indicated mostly quartz (~90%), with few dark fragments
40-45	***100% recovery***

40-45	Fine to lower medium sand; darker spots from 40-41.6 ft
45-50	***100% recovery***
45-46.85	Fine to lower medium sand (maybe some upper medium)
46.85-48.18	Fine to medium sand; darker brown color
48.18-49.5	Fine sandy clay
49.5-50	Clay, hard, with some fine sand (less than above)

OU-4 Core #1

Depth (ft)	Description
0-5	***54% recovery***
2.3-3	Dark, clayey topsoil
3-5	Very fine to fine sand, occasional organics (roots)
5-10	***66% recovery***
6-6.6	Very fine to fine sand, occasional organics (roots)
6.6-7.5	Fine sand, transitioning to medium sand
7.5-9.3	Medium sand, clean; mostly quartz
10-15	***100% recovery***
10-11.5	Fine to medium sand
11.5-12.5	Medium sand
12.5-13	Fine sand
13-13.5	Clayey fine sand
13.5-15	Clay with silt or very fine sand; sticky; ribbons poorly
15-20	***76% recovery***
16-16.6	Clay with silt or very fine sand
16.6-19.8	Clay, sticky, gray-brown, some brown zoning
20-25	***96% recovery***
20-20.5	Clay with fine sand
20.5-23	Clay, sticky, gray-brown
23-24.8	Clay, sticky, transitioning to reddish-brown
25-30	***98% recovery***
25-29.9	Clay, sticky, with laminations/layers of clay with trace very fine sand; Clay with sand found from 25-25.4 ft, 24.9-25 ft, 27.1-27.3 ft, and 28.7-28.9 ft
30-35	***0% recovery; sleeve stuck in pipe***
	Sand at bottom of plug (probably medium); appeared to be all sand falling out of sleeve

OU-4 Core #2

Depth (ft)	Description
0-5	***72% recovery***
1.4-2.1	Dark topsoil
2.1-2.9	Very fine to fine sand
2.9-5	Transitions to medium sand; some fine, dark laminations with slight yellow to red changes
5-10	***100% recovery***
5-5.4	Fine to medium sand; few organics (possibly sluff)
5.4-9.2	Medium sand, clean
9.2-10	Clay with trace very fine sand
10-15	***98% recovery***
10-10.7	Fine to medium sand
10.7-12	Medium sand
12-14.9	Clay with silt or very fine sand
15-20	***98% recovery***
15-17.4	Clay with silt; ribbons poorly
17.4-19.9	Clay, sticky, buff brown with some reddish-brown zoning
20-25	***98% recovery***
25-29.9	Clay, sticky; some brown/reddish-brown color zonation and possible laminations visible
25-30	***98% recovery***
25-25.9	Clay with very fine sand
25.9-26.2	Clay, sticky, with brown/reddish-brown color zonation
26.2-26.7	Clay with silt or very fine sand
26.7-29.4	Clay, sticky, with brown/reddish-brown color zonation
30-35	***68% recovery***
31.6-32.1	Fine to medium sand
32.1-35	Medium sand, clean, quartz; darker sand from 34-35 ft
35-40	***90% recovery; sleeve stuck so lost some off both ends***
35.4-39.9	Medium sand, some dark spots (organics?); 15mm diameter Limestone Pebble at 39 ft
40-45	***34% recovery; sleeve stuck so only grab sample from bottom***
43.3-45	Medium sand
45-50	***68% recovery; sleeve stuck so lost some off both ends***
46.5-47.2	Clay with very fine sand (sluff?)
47.2-48	Fine to medium sand
48-49.9	Fine sand with clay
50-53	***100% recovery; note only drilled to 53 ft***
50-51.2	Clay with silt or very fine sand
51.2-52.8	Fine sand or silt with clay
52.8-53	Clay, sticky, brown

APPENDIX D: Hydrostratigraphic Model Design

To create the hydrostratigraphic models several steps had to be performed. First, a model grid was defined. Then 80 training images were created, with a subset of these selected for use in the *snesim* algorithm. Finally, hard data were imported and parameters were defined and analyzed during the running of the *snesim* algorithm. Details of this process are described in the following sections.

Model Grid and Layers

The size of the area in Outagamie County to be modeled (Fig. 1) is approximately 22.5 miles (E-W) by 16 miles (N-S). The size of the grid was based on data from the WCRs and ERI. The horizontal spacing was chosen to be 1200 x 1200 ft, in order to allow for small enough grid spacing to account for horizontal sand body lengths identified from the ERI and to keep the hydrostratigraphic model from being too large and thereby increasing computational time. Since sand was present along the entire length of each of the ERI transects, ranging from approximately 375 to 650 ft, with no indication of pinching out near the ends of the transect, it can be assumed that a slightly larger grid spacing is an approximate minimum size for the sand bodies. The vertical spacing was chosen to be 5 ft because the mode thickness from the WCR analysis for the high K units was 10 ft, allowing for units to be thinner than the mode. The model grid has 99 cells in the x-direction (E-W), 71 cells in the y-direction (N-S), and 160 layers, for a total of just over 1.1 million nodes.

Training Image Creation & Selection

SGeMS TIGENERATOR was used to create 80 training images, of which 12 were selected for use in the creation of the hydrostratigraphic models with the *snesim* algorithm. The TIGENERATOR generates shapes to represent the pattern distribution of a depositional environment using a non-iterative, unconditional Boolean simulation. This is basically an object generator, which places a set of objects that are not constrained to local data onto a grid. Parameters that have to be defined to create a training image include geobody type, proportion, geobody interaction, and geobody parameters. Eight parameter sets were chosen, with 10 realizations for each, for a total of 80 training images.

Geobody type is basically a shape, and can be sinusoid, ellipsoid, half-ellipsoid, or cuboid. One or more types can be used for each parameter set. Shapes were based on the depositional environment, as well as visual comparison of the training images to the WCR data shown in Figure 4. The first four training image parameter sets were each run with a different set of geobodies. Visual examination excluded two of them (cuboid/sinusoid, ellipsoid/half-ellipsoid), as geologically unreasonable and a combination of visual examination and lack of data for added complexity excluded a third (lower half-ellipsoid/ellipsoid/sinusoid). A realization for each of these is shown in Figure D1. The remaining three training image parameter sets were then run with the selected geobodies (lower half-ellipsoid/sinusoid) that were judged to best represent the likely depositional environment of underflow type deposits (gravel) and beach deposits (sand).

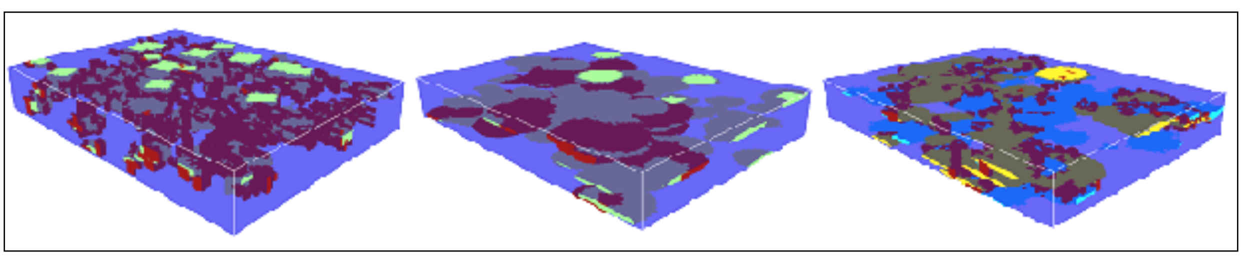

Figure D1. Training images from the geobody types not selected due to visual examination lack of comparison to WCRs in 3-D and geologic plausibility. From left to right the geobodies used are cuboid/sinusoid, ellipsoid/half-ellipsoid, and lower half-ellipsoid/ellipsoid/sinusoid.

Proportion is the total volume that a geobody type should fill. A proportion of 0.2 (20%) was used for each parameter set based on the calculated percent by thickness from the WCRs (high K units were 19.5%). Because sand was present along the entire length of each of the ERI transects, it is likely the thickness can be projected into volume.

Geobody interaction is the way the second or subsequent geobodies are placed in space with regards to the previous geobodies, and includes three parameters: erosion, minimum overlap, and maximum overlap. All geobodies erode the background, but have the option to either erode or be eroded by previously simulated geobodies. Seven of the eight parameter sets were set to erode the previous geobodies, as during the last glaciation the ice sheet would have advanced and retreated several times, eroding some of the earlier deposits and then depositing other sediment. Minimum and maximum overlap constrains the fraction of volumetric overlap between two geobodies. For seven of the eight parameter sets a minimum of 0.01 and maximum of 0.8 was used, allowing for geobodies to be "deposited" above previous geobodies. The eighth parameter set used a minimum of zero to allow the geobodies to either be deposited or not deposited above the previous geobodies. However, this causes the placement of subsequent geobodies to be more random, resulting in training images that are not representative of the depositional environment.

Geobody parameters are assigned for each geobody type and include orientation and dimensions (dependent on geobody type). The parameters can be defined as constant (mean), uniform (minimum, maximum), or triangular (minimum, mode, maximum). Orientation is the direction in which the geobody is "deposited". Since the ice sheet moved in a east-northeast direction (Clark *et al*., 2008), the deposits will generally be oriented in the same direction as the ice sheet; thus, a triangularly defined orientation was used for all geobody types in every parameter set of 15, 45, 95 (in degrees). The maximum orientation was extended to be approximately due south since in Outagamie County the curvature of the edge of the ice sheet was such that not all deposits coming off the ice sheet were necessarily deposited in the overall ice sheet direction. Dimensions are defined by number of nodes, and were based on information from the WCR analyses, ERI, and the depositional environment. Table D1 lists the dimensions used for the eight training image parameter sets.

Selection of the training images was based on visual comparison with the 3-D WCR display and general geologic plausibility. Of the 80 images, 12 were selected to be run with the *snesim* algorithm (Fig. D2). Note that these 12 were realizations from only four of the eight training image parameter sets; specifically training images 3, 5, 6, and 7 (Table D1).

Hard Conditioning Data

The hard conditioning data for the hydrostratigraphic models are mainly from the WCRs, but also include well reports from previously drilled rotosonic boreholes (Hooyer *et al*., 2008). The data must be in point form for multiple-point geostatistics; thus, the center point of each unit was taken as a data point. For example, if clay were present from 700-720 ft elevation, the hard data point would be clay at 710 ft elevation. The total number of hard data was 5,153. During simulation, the hard data are assigned to the nearest grid node and kept constant.

Table D1. Dimensions for geobodies used in the training image generator. Ten realizations were run for each training image. Dimensions are listed as constant, uniform, or triangular (1, 2, or 3 values; see above text for explanation) and in number of nodes (not length measurements). Maxrad, medrad, and minrad, are the maximum, median, and minimum radii for ellipsoid objects. For sinusoidal objects thick is thickness, amp is amplitude, and wave is wavelength.

Training Image	Geobody Type	Geobody Dimensions
1	cuboid	Length 1,10; Width 1,10; Height 1,2,40
	sinusoid	Length 1,4; Width 1,2; Thick 1,2,40; amp 2; wave 2,15
2	ellipsoid	Maxrad 2,10; medrad 1,10; minrad 1,2,40
	lower half-ellipsoid	Maxrad 2,10; medrad 2,10; minrad 1,2,40
3	lower half-ellipsoid	Maxrad 2,10; medrad 2,10; minrad 1,2,40
	sinusoid	Length 1,4; Width 1,2; Thick 1,2,40; amp 2; wave 2,15
4	lower half-ellipsoid	Maxrad 2,10; medrad 2,10; minrad 1,2,40
	ellipsoid	Maxrad 2,10; medrad 1,10; minrad 1,2,40
	sinusoid	Length 1,4; Width 1,2; Thick 1,2,40; amp 2; wave 2,15
5	lower half-ellipsoid	Maxrad 2,10; medrad 2,10; minrad 1,2,40
	sinusoid	Length 1,4; Width 1,2; Thick 1,2,40; amp 1,3; wave 2,4
6	lower half-ellipsoid	Maxrad 2,10; medrad 2,10; minrad 1,2,40
	sinusoid	Length 1,4; Width 1,2; Thick 1,2,40; amp 1,3; wave 2,4
7	lower half-ellipsoid	Maxrad 2,5; medrad 2,5; minrad 1,2,40
	ellipsoid	Length 1,4; Width 1,2; Thick 1,2,40; amp 2; wave 2,15
8	lower half-ellipsoid	Maxrad 2,10; medrad 2,10; minrad 1,2,40
	ellipsoid	Length 1,4; Width 1,2; Thick 1,2,40; amp 2; wave 2,15

Parameters Analyzed

Certain parameters were kept the same for all *snesim* simulations, while others were varied in addition to varying the training image used. Using the 12 selected training images (Fig. D2), 30 simulations were run, with 10 realizations for each, for a total of 300 hydrostratigraphic models. Eight of the simulations were run with the same training image but varying other parameters. After analysis of the effects of these parameters, the remaining simulations were run with the other 11 selected training images.

Liu (2006) performed sensitivity analyses on many of the *snesim* input parameters using a 2-D case. Although the models for this research are in 3-D, many of the 2-D results can be extended into 3-D. A correction factor, named the servosystem correction, is used to bring the simulated target proportion closer to the target, but this loses structural information from the training image. The servosystem parameter must be set between 0 and 1, with higher values causing a larger correction to the target proportion. For all simulations in this research the servosystem parameter was set to 0.5, to allow a balance between the training image geometry and the target proportion. The target distribution itself was one of the parameters that was tested as will be described below. Liu (2006) determined that the program was not very sensitive to the minimum number of replicates parameter, and an empirical value between 10 and 20 should be used, with a smaller value needed for increasing number of multi-grids (discussed below). Thus a value of 10 was used for all simulations in this research. Liu (2006) also analyzed the search template geometry, and determined it was most robust to use an isotropic search ellipsoid. The size of the ellipsoid was tested, but all were horizontally isotropic (circle). Since the z-direction is of a much shorter length, a fully isotropic search ellipsoid is impractical. The final parameter that was tested for this research was the number of multi-grids. Multi-grids allow for large scale structures to be simulated by first simulating nodes on the coarsest grid with a large rescaled template, then simulating nodes on the second coarsest grid with a smaller rescaled template, and so on until the finest grid is simulated using the original template. Liu (2006) found that increasing the number of multi-grids to 5 and 6 does not improve large scale structure, and only having 1 multi-grid is unacceptable as it only captures small-scale structures.

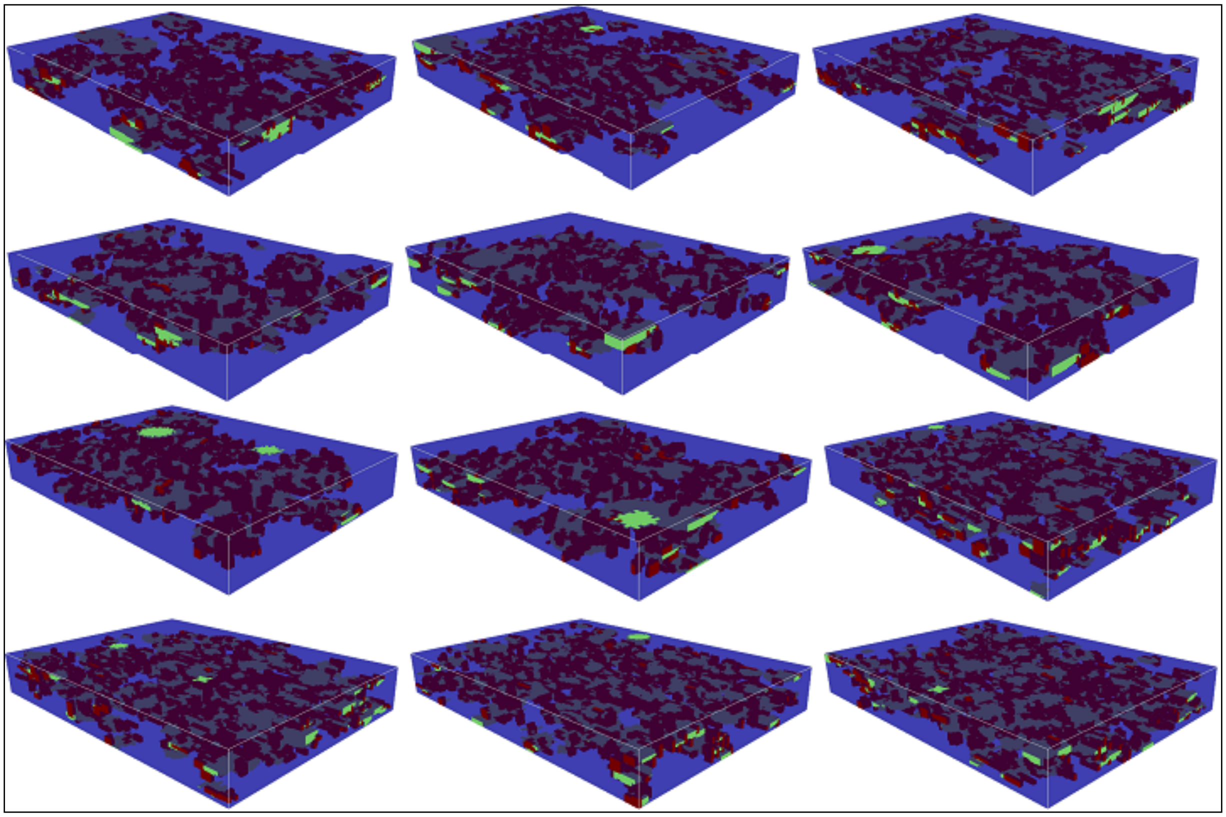

Figure D2. The twelve training images selected for use in the *snesim* algorithm.

Three parameters were tested by running simulations with the same training image. These parameters are the target marginal distribution (or proportion), the size of the search template, and the number of multi-grids. As described in the introduction, the percent by thickness for the units was approximately 20% for the high K units, so this value was used for the proportion in the hydrostratigraphic model. However, one model was tested with a lower percentage of 10%. The two sets of tested values for the target marginal distribution (given as a ratio) for low K units, sand, and gravel, respectively, are as follows: 0.8, 0.1, 0.1 and 0.9, 0.05, 0.05. Analysis of connectivity statistics (see Appendix F for more information) indicated similar connectivity despite having a lower percentage (10%) of high K material; thus, 20% was used. Furthermore, the values of 0.8, 0.1, 0.1 were used for the remaining models as these are the values suggested by the WCR data. Two sizes of search template were tested, with values in feet in the x, y, and z directions, respectively, as follows: 12000, 12000, 50 and 24000, 24000, 100. Analysis of connectivity statistics indicated slightly higher connectivity in the second of the two templates, which is not surprising given that Liu (2006) found that the search template size should be adapted to the dimensions of the structures. Since the maximum size of these sand bodies is unknown, the smaller size of 12000, 12000, 50 was used for all other simulations so as to not add additional connectivity that may not be present. Finally, the number of multi-grids was tested by running models with 1 through 5 multi-grids. Connectivity statistics showed little change in connectivity with models using 1, 2, or 3 multi-grids. However, visually the models with 1 or 2 multi-grids were not geologically plausible as they only captured small structures (Fig. D3). Connectivity statistics changed with 4 multi-grids, indicating greater connectivity in the z-direction and fewer, but longer connected pathways. Additionally, the average proportion of high K units increased slightly from 0.17 to 0.18. When 5 multi-grids were used this proportion increased to 0.19, with even fewer and longer pathways. However, the connectivity in the z- and y-directions actually decreased, while x-direction connectivity increased. Additionally, the models visually began to have structures that were too large, particularly near the surface; thus, only 3 and 4 multi-grids were used in the other simulations.

Statistics from all 300 models were imported into an Excel file and analyzed. Results from initial simulations with the same training image aided in the determination of parameters (as described above) used in later simulations. Of the 300 models, 240 have acceptable parameters as discussed above and were considered in the selection process. Table D2 displays the averages, standard deviations, and maximum and minimum values for all 300 models and also the subset of 240 acceptable models.

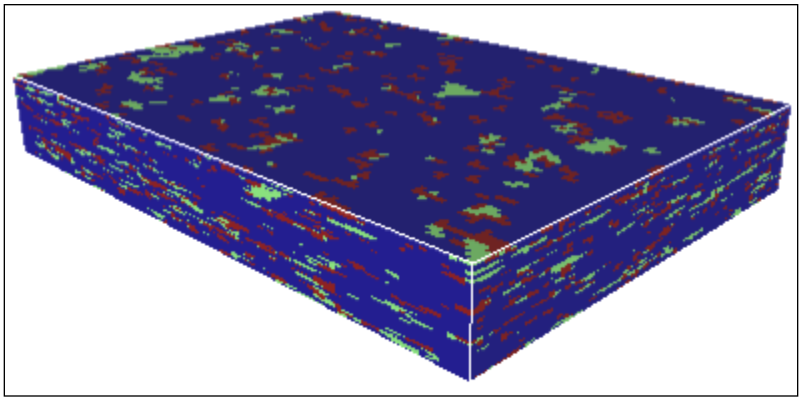

Figure D3. Hydrostratigraphic model using only 1 multi-grid. Note the lack of large scale structures.

Table D2. Average (AVG), standard deviation (SD), maximum value (MAX) and minimum value (MIN) for all 220 models (all) and the subset of 240 models with acceptable parameters (okpar). Note that the pixel size is 1200 ft in the x and y directions, and 5 ft in the z direction.

Model	Proportion	Number of connected components	Mean size (pixels)	Mean length-x (pixels)	Mean length-y (pixels)	Mean length-z (pixels)
AVG_all	0.16	10971	17.68	1.50	1.52	3.28
SD_all	0.02	2038	4.89	0.08	0.08	0.33
MAX_all	0.19	15274	31.49	1.69	1.69	4.47
MIN_all	0.09	6673	6.77	1.28	1.29	2.37
AVG_okpar	0.16	11192	17.31	1.51	1.53	3.34
SD_okpar	0.01	1942	4.42	0.07	0.07	0.29
MAX_okpar	0.19	15209	30.89	1.69	1.69	4.47
MIN_okpar	0.14	6824	10.23	1.30	1.34	2.69

Model	Max size (pixels)	Max length-x (pixels)	Max length-y (pixels)	Max length-z (pixels)	Min size (pixels)	Min length-x (pixels)	Min length-y (pixels)	Min length-z (pixels)
AVG_all	105352	57.95	71.00	160.00	1.00	1.00	1.00	1.00
SD_all	27437	22.00	0.00	0.00	0.00	0.00	0.00	0.00
MAX_all	177015	99.00	71.00	160.00	1.00	1.00	1.00	1.00
MIN_all	45400	29.00	71.00	160.00	1.00	1.00	1.00	1.00
AVG_okpar	104107	53.99	71.00	160.00	1.00	1.00	1.00	1.00
SD_okpar	23226	19.02	0.00	0.00	0.00	0.00	0.00	0.00
MAX_okpar	177015	99.00	71.00	160.00	1.00	1.00	1.00	1.00
MIN_okpar	66215	35.00	71.00	160.00	1.00	1.00	1.00	1.00

Model	Number of percolating components-x	Number of percolating components-y	Number of percolating components-z
AVG_all	0.16	1.36	1.55
SD_all	0.37	0.51	0.71
MAX_all	1.00	3.00	5.00
MIN_all	0.00	1.00	1.00
AVG_okpar	0.10	1.36	1.58
SD_okpar	0.29	0.50	0.72
MAX_okpar	1.00	3.00	5.00
MIN_okpar	0.00	1.00	1.00

APPENDIX E: CONNEC3D Overview

All 300 hydrostratigraphic models were analyzed for connectivity statistics using CONNEC3D (Pardo-Igúzquiza & Dowd, 2003), which calculates a number of connectivity statistics and writes these to several output files. This free program was used as a post-processor by de Vries et al., (2009) to create training images with all channel features connected, and Pardo-Igúzquiza & Dowd (2003) demonstrated its capabilities with a randomly generated model, but it has not been used as a quantitative measure of connectivity with a model created from field data.

Two input files need to be written for CONNEC3D (Pardo-Igúzquiza & Dowd, 2003). First the hydrostratigraphic model output must be categorized into two units based on a threshold value of K so that all high K values (sand and gravel bodies) are assigned a value of 1 and all low K values (glacio-lacustrine and till deposits) are assigned a value of 0. This information must be saved as a .dat file. The other input file is a nine-line parameter file containing the names of the .dat file and output files, the grid size and spacing, and two adjustable parameters: connectivity analysis and lag. The connectivity analysis is the number of adjacent cells used in the determination of the connectivity statistics (Fig. E1) and can be either 6 (defined by cells that share a face), 18 (defined by cells that share a face or an edge), or 26 (defined by cells that share a face, edge, or vertex). The lag is the number of cells over which the connectivity statistics are calculated in any direction. All hydrostratigraphic models were run with a connectivity analysis of 18 and a lag of 30 cells.

The program calculates the following connectivity statistics: proportion of unit that is being analyzed (high K units for this research), number of connected components, mean size of a connected component (cc), mean length in the x, y, and z directions of a cc, size of the largest and smallest cc, length in the x, y, and z directions of the largest and smallest cc, and number of percolating components in the x, y, and z directions. A percolating component is a single connected component that connects from one end to the other in a specific direction, for example a percolating component in the z-direction would indicate a connected pathway from the top to the bottom of the model. Additionally, the connectivity function (for this research estimated by the number of high K cells within the lag distance that are connected divided by the total number of high K cells within the lag distance) is calculated for 13 directions (x, y, z, four 3-D diagonals, and six diagonals of planes). Also the average of the x, y, and z directions and the average of the four 3-D diagonals are calculated.

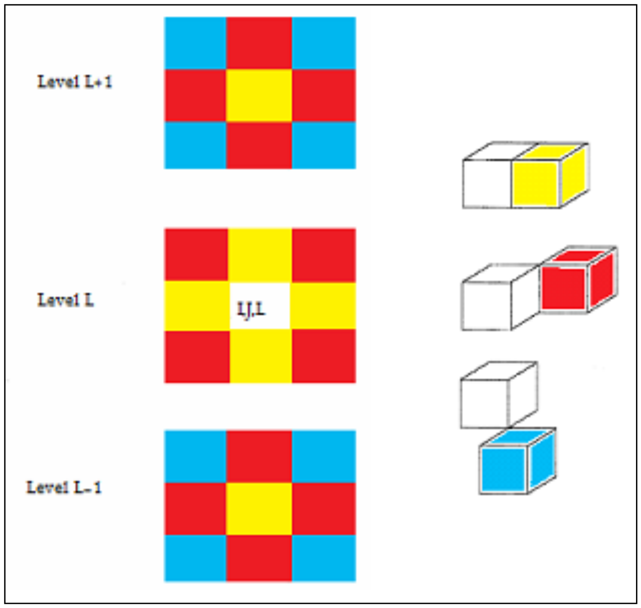

Figure E1. Connectivity analysis demonstrated for cell I,J,L (on left). Shown are the six neighbors of 6-connectivity analysis (yellow), 18 neighbors of 18-connectivity analysis (yellow plus red) and 26 neighbors of 26-connectivity analysis (yellow plus red plus blue). On the right: face (yellow), edge (red), and vertex (blue) connectivity are demonstrated with two nodes. Adapted from Pardo-Igúzquiza & Dowd (2003).

APPENDIX F: Selection of Representative Set of Models

A representative set of models was selected from the 240 models with acceptable parameters, based on analyses of the connectivity statistics. Several of the statistics, such as the minimum size and lengths in all directions had a standard deviation of zero and were not considered in selecting a representative set. Three of the connectivity statistics had variability that needed to be considered in selecting models: proportion, number of connected components, and maximum size in pixels.

The overall range of each of these three statistics was analyzed graphically (Figs. F1-F3). As the proportion of high K material increases (Fig. F1), the number of connected components decreases (Fig. F2), indicating that there are fewer but longer connected pathways. Additionally, there is some correlation with the longest maximum size (in pixels; Fig. F3) occurring for those models having fewer connected components, further indicating that fewer but longer pathways are generally occurring in these models.

In addition to the graphical analysis, every model was analyzed for each of these connectivity statistics and assigned a categorical value of three letters based on the value of each individual statistic. Each statistic was assigned a range for low (L), average (A), and high (H) values (Table F1). Then each model was categorized based on its statistics for proportion, number of connected components, and number of percolating components. For example, a model with low values for each of these would be categorized as an LLL model.

The final selection took into account the overall range of the three statistics and the categorical values of all the models, as well as ensuring selection of models with different training images and number of multi-grids (3 & 4). Additionally, the number of percolating components in the x-, y-, and z-directions and the maximum length in the x-direction were considered. After analysis of all of these factors, six models were selected as a representative set.

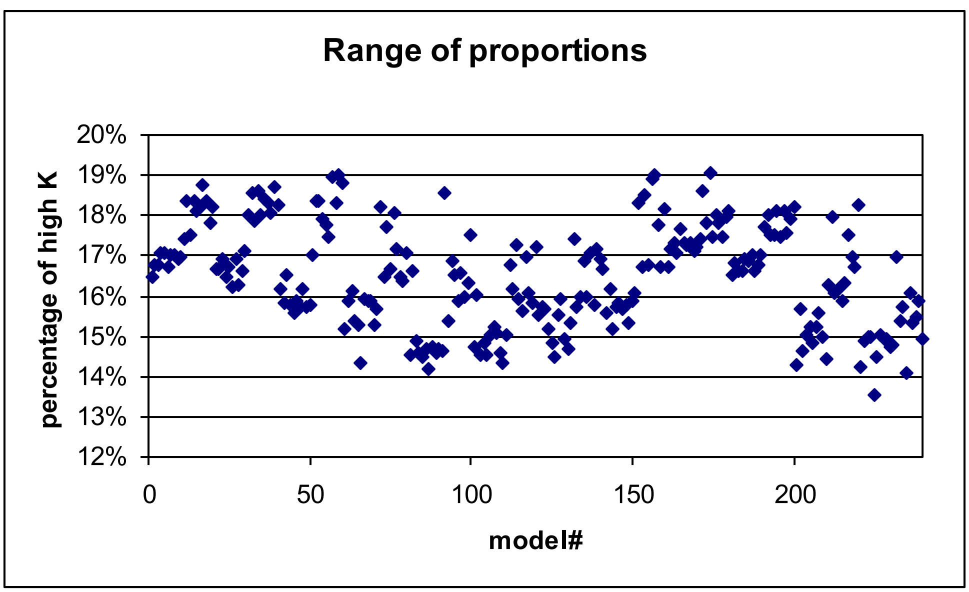

Figure F1. Proportion values for the 240 models. Note that although the proportion was set at 20% for the simulations, the simulated values vary from approximately 13.5-19% due to the servosystem correction being set at 0.5, which allows for the training image geometry to also be observed.

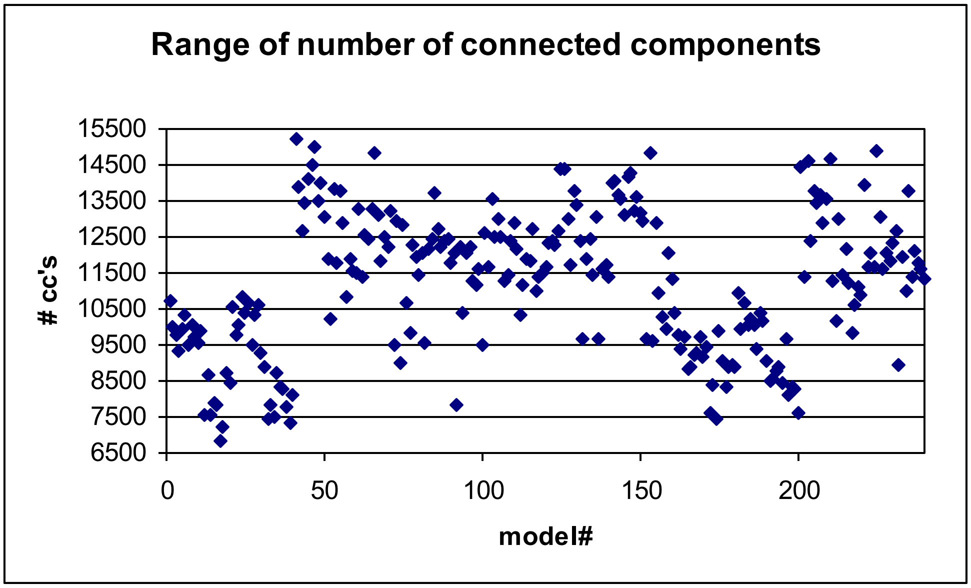

Figure F2. The number of connected components for the 240 models. Note that the model number is the same for the proportion graph (Fig. 2.9), and comparison indicates generally fewer connected components with increasing proportion (i.e., models 1-40, 161-200)

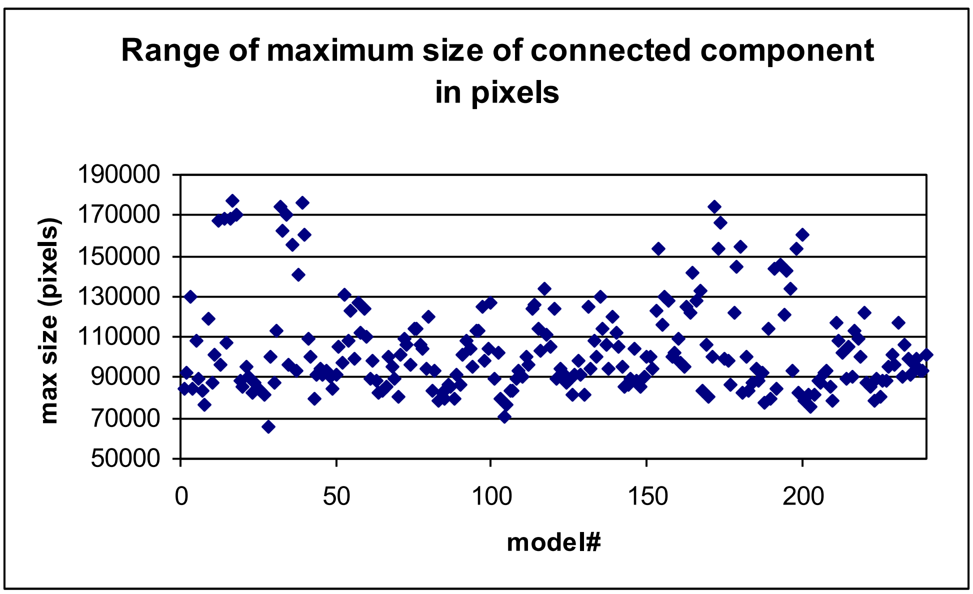

Figure F3. Values of maximum size of connected components measured in pixels for the 240 models.

Table F1. Values for each statistic that were used to assign low, average, and high ranges to each model.

Statistic	Low	Average	High
proportion	<0.155	0.155-0.175	>0.175
number of connected components	<10000	10000-12000	>12000
maximum size of connected component (pixels)	<90000	90000-115000	>115000

Initial analyses were based on the categorical values for the models. Certain categories, such as LLL, LLA, and LLH did not have any models. For other categories, including LHL and AHA, over 10% of the models fit in this category. Through analysis of the percentage of each category, and taking into account that models of categories with only one difference in letter (e.g. HAA and HAH) were often identical in the two categories with only a minor difference in the third, it was determined that five to seven models would be necessary for a representative set.

Selecting the representative set, including determining the exact number necessary, was done iteratively. One model was selected for a category with a high percentage, then a second selected from another category, until five to seven models were selected. Throughout the process each set of models was compared for number of multi-grids and training images, as well as insuring that individual values for the three statistics represented the full range of values. Certain sets would not work because more than one model would be from the same training image, or all of the models would be realizations from the same training image parameter set. Eventually, the six selected models were determined through this process. Figures F4-F6 graphically show that the selected models represent the range of each of the connectivity statistics. Figure F7 demonstrates that the selected models represent the range of models based on the 27 possible categories (e.g., LLL). Graphs for the connectivity function in the x, y, and z directions indicate a range of connectivities are represented by these models (Figs. F8-F10). Table F2 displays statistics for each of the selected models, as well as the averages of these statistics compared to the averages of the 240 acceptable models. These figures and tables demonstrate that the six selected models truly are a representative set. Finally, Figure F11 shows a 3-D image of each of the selected models.

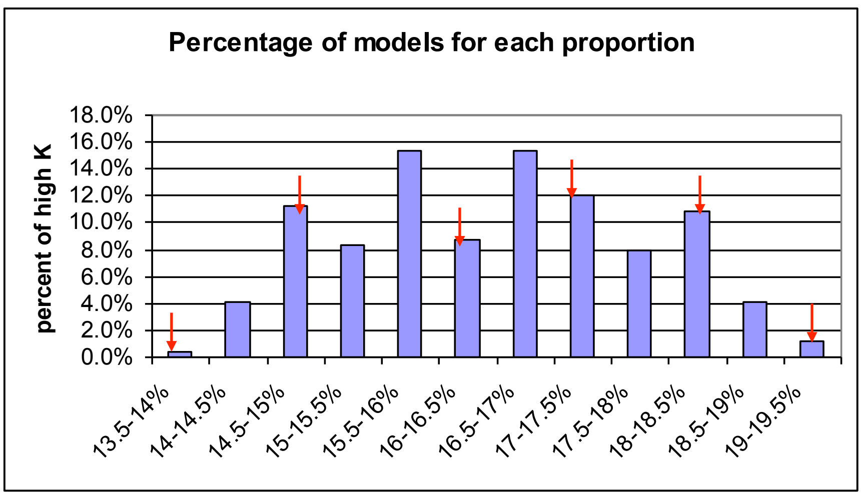

Figure F4. Percentage of models for each proportion (listed as percent by volume). The red arrows indicate the proportion of the six selected models.

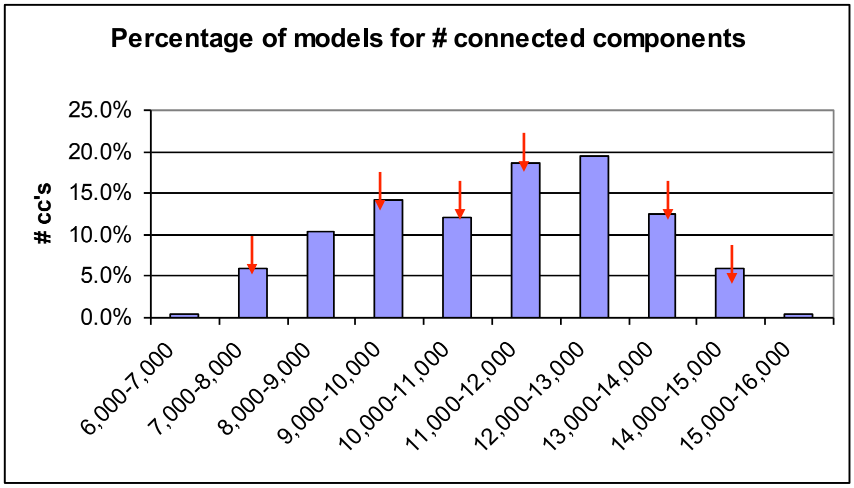

Figure F5. Percentage of models for number of connected components. The red arrows indicate the number of connected components of the six selected models.

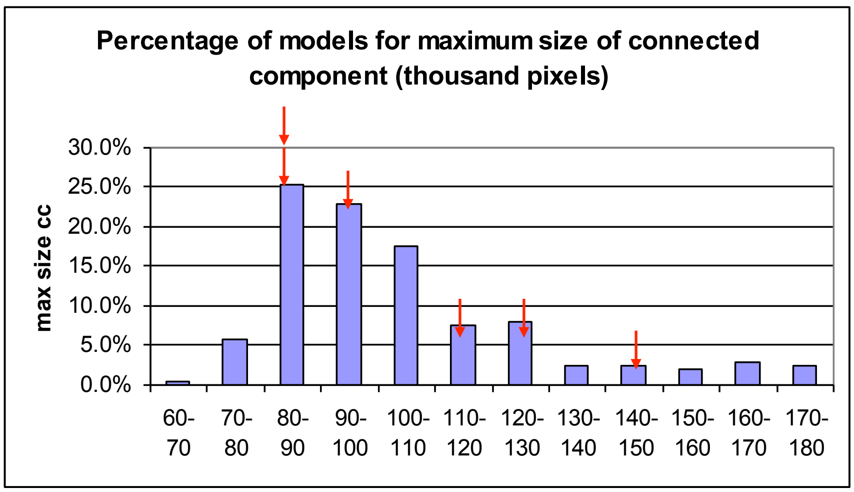

Figure F6. Percentage of models for maximum size of connected component (in thousands of pixels). The red arrows indicate the maximum connected component size of the six selected models.

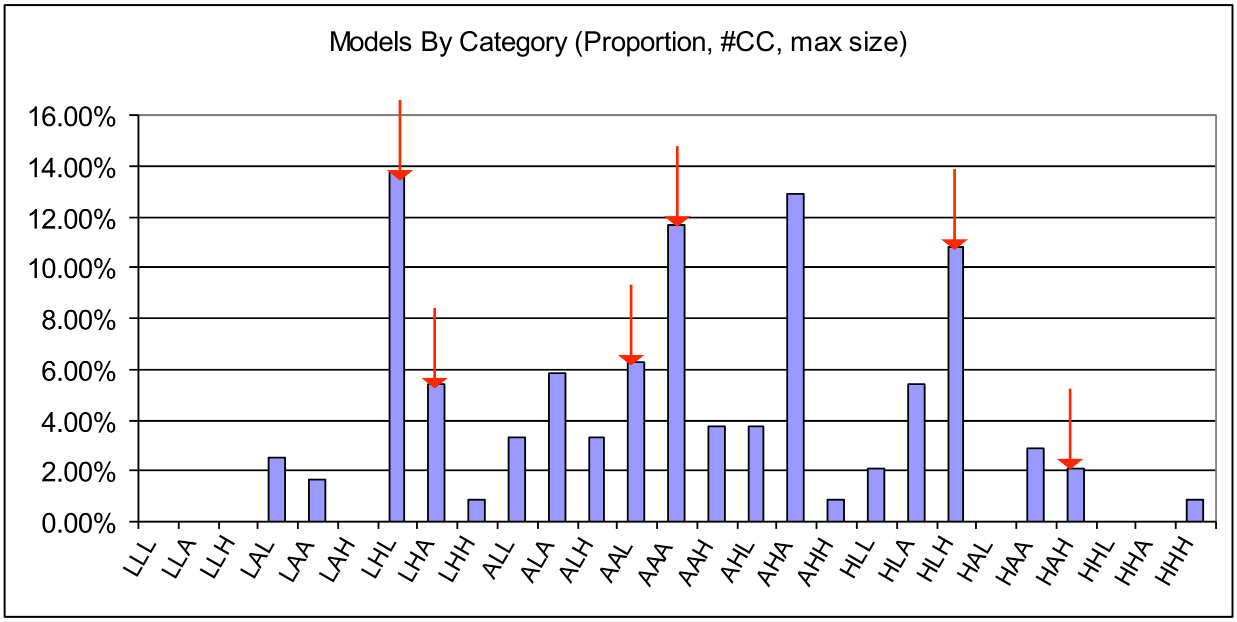

Figure F7. Percentage of models by category (see text and table F1 for details). The red arrows indicate the category of the six selected models.

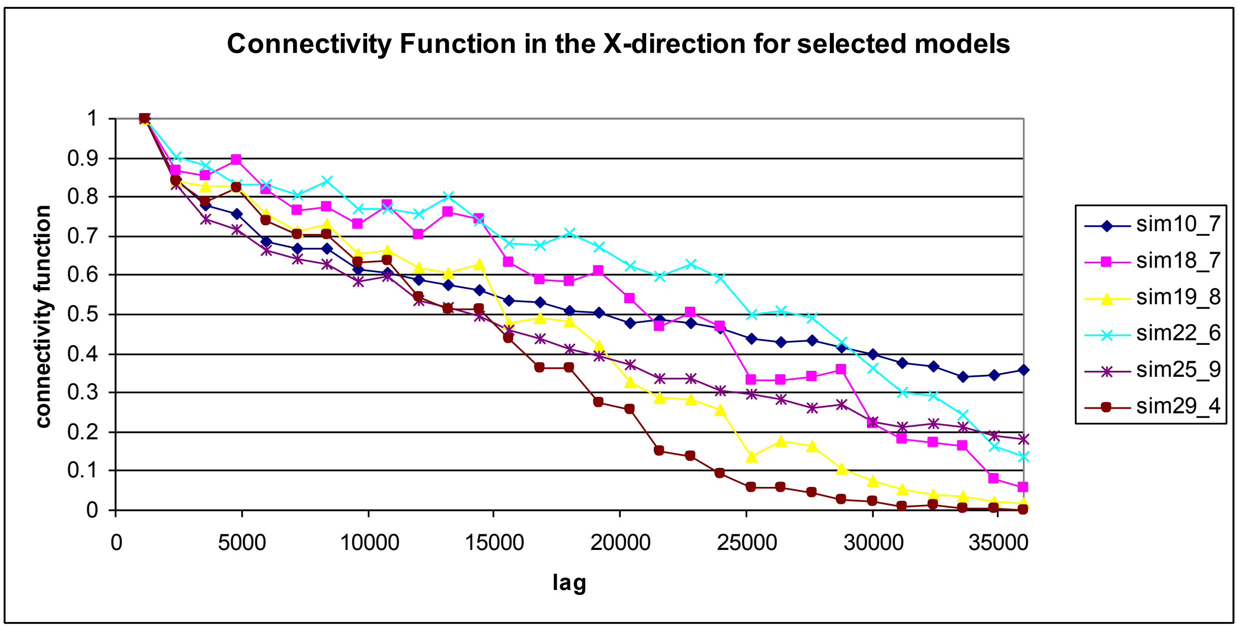

Figure F8. Connectivity function (number of connected high K cells within the lag distance / total number of high K cells within the lag distance) in the x-direction for each of the selected models. Model sim10_7 has a percolating component in the x-direction, and thus maintains a higher connectivity function at larger lag distances.

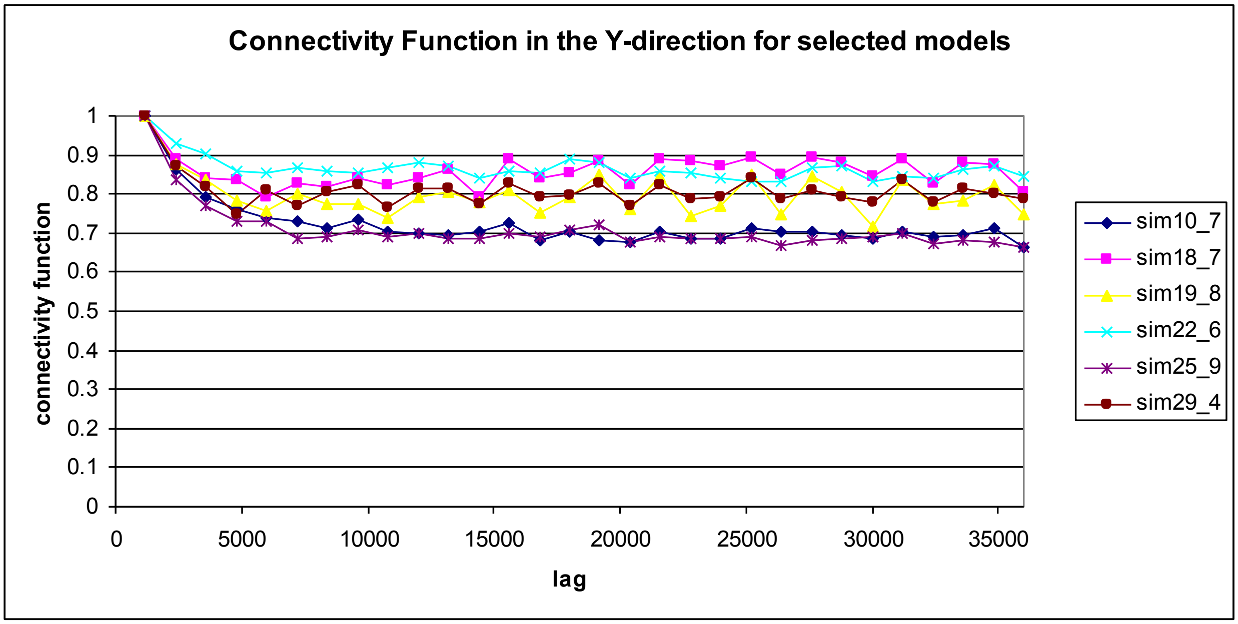

Figure F9. Connectivity function (number of connected high K cells within the lag distance / total number of high K cells within the lag distance) in the y-direction for each of the selected models.

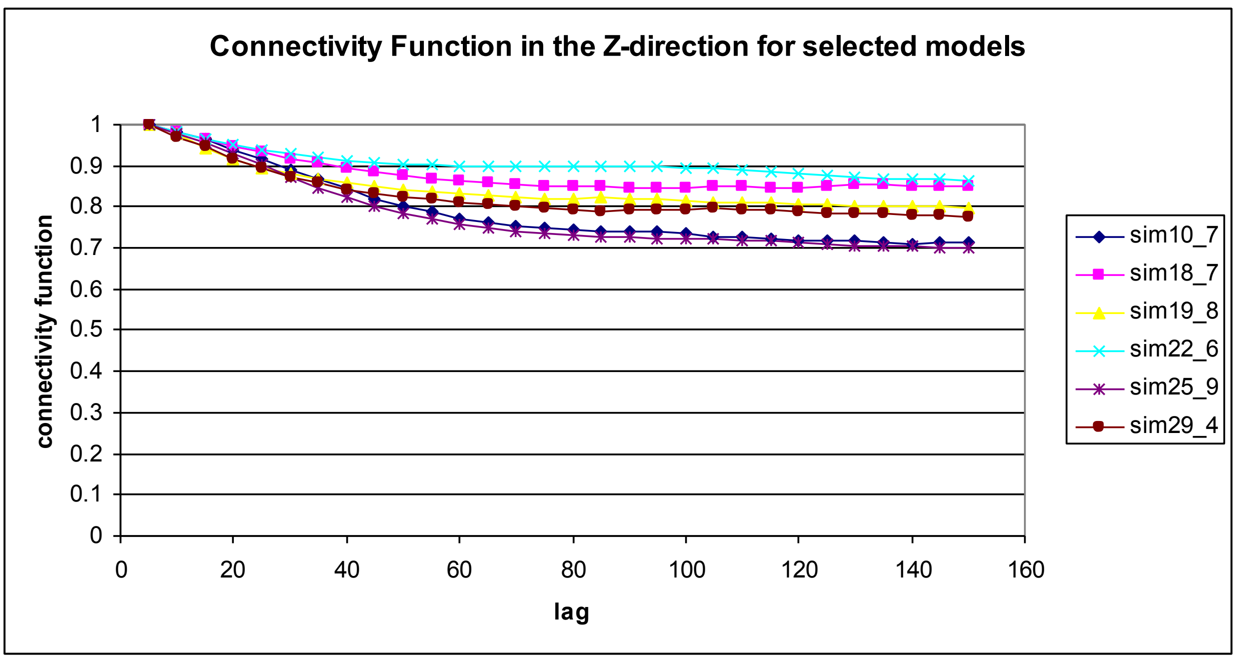

Figure F10. Connectivity function (number of connected high K cells within the lag distance / total number of high K cells within the lag distance) in the z-direction for each of the selected models.

Table F2. Selected models and their corresponding training image (TI), number of multi-grids, and connectivity statistics that did not have a standard deviation of zero for all models. The last two rows list the average of these statistics for the selected models and the 240 possible models. Note that the averages of the representative set are nearly identical to those of all the possible models. Model names are given by simnumber_realization number and training images by training image number_realization number. Pixel size is 1200 ft in the x and y directions, and 5 ft in the z direction.

Model	TI	# multi-grids	proportion	#cc's	Mean size (pixels)	Mean length-x (pixels)	Mean length-y (pixels)	Mean length-z (pixels)
sim10_7	7_2	4	0.1808	7753	26.2326	1.5184	1.5443	3.2602
sim18_7	3_3	4	0.1607	11406	15.8407	1.3839	1.4295	3.8511
sim19_8	5_6	3	0.1492	13800	12.1569	1.5143	1.5214	3.2954
sim22_6	6_6	4	0.1903	10274	20.8331	1.4963	1.5742	3.0993
sim25_9	7_1	3	0.1703	9052	21.1548	1.5166	1.5104	3.1130
sim29_4	3_9	3	0.1352	14868	10.2273	1.4531	1.4875	3.1776
AVG-selected			***0.16***	***11192***	***17.74***	***1.48***	***1.51***	***3.30***
AVG-all plausible (240)			***0.16***	***11192***	***17.31***	***1.51***	***1.53***	***3.34***

Model	Max size (pixels)	Max length-x (pixels)	# perc comp-x	# perc comp-y	# perc comp-z
sim10_7	140420	99	1	1	1
sim18_7	110996	42	0	1	3
sim19_8	91895	41	0	1	1
sim22_6	127871	40	0	2	2
sim25_9	79940	56	0	2	2
sim29_4	80439	37	0	1	1
AVG-selected	***105260***	***53***	***0.17***	***1.33***	***1.67***
AVG-all plausible (240)	***104107***	***54***	***0.10***	***1.36***	***1.58***

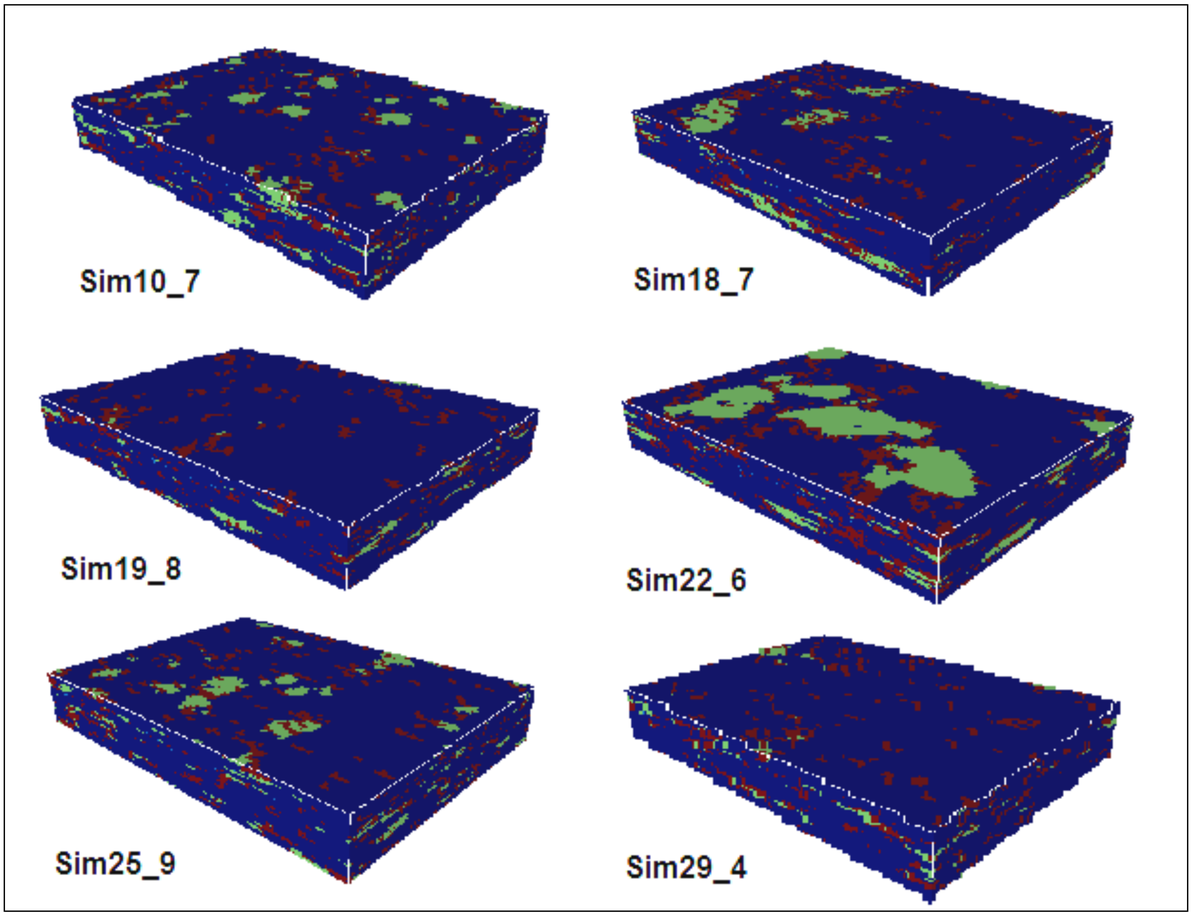

Figure F11. Selected models, names for each are to the bottom left corner of the model and correspond to those listed in Table F2. The view shows the southern and eastern edges of the model on the left and right sides, respectively. Red and green (sinusoids/sand and lower-half ellipsoids/gravel, respectively) are the high K units.

APPENDIX G: Groundwater Flow and Transport Models

Model Design

Regional groundwater flow in Outagamie County is mainly to the east (Fig. G1). However, in the glacial Lake Oshkosh sediment, flow is mainly vertical (Hooyer *et al.*, 2008). As will be described in more detail in this appendix, the model grid and boundary conditions have been adjusted to simulate this vertical flow.

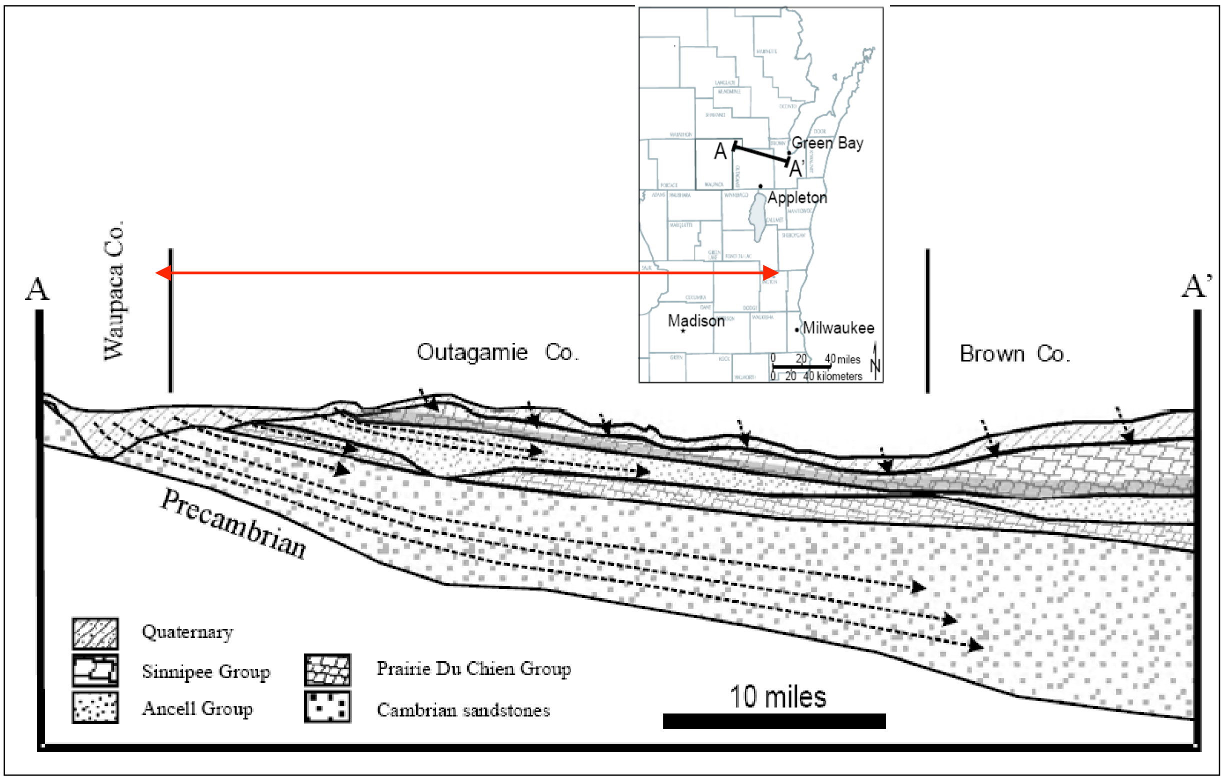

Figure G1. Idealized cross section showing the bedrock units and groundwater flow in the study area (Outagamie Co.). General location of the cross section is shown in the inset. Red arrow indicates approximate extent of groundwater flow models in the direction of the cross-section. (from Hooyer *et al.*, 2008)

Model Grid & Layers

The Lake Michigan Basin Model (LMBM, Feinstein *et al.*, 2010), which has horizontal grid spacing of 5,000 by 5,000 feet in the area of interest and 20 layers of variable thickness, was initially used to define the Outagamie County groundwater flow models using the telescopic mesh refinement (TMR, Ward *et al.*, 1987) option in Groundwater Vistas. The groundwater flow models have the same uniform horizontal grid spacing (1,200 by 1,200 feet, with 71 rows and 99 columns) as the hydrostratigraphic models. Except for layer 1, the 98 layers in the groundwater flow models have uniform thickness of 5 ft, which is the same as the hydrostratigraphic models. The top twenty layers of the hydrostratigraphic models were removed because they were either above the maximum land surface elevation or the maximum water table elevation. The bottom sixteen layers of the hydrostratigraphic models were also removed because they are entirely within the Precambrian bedrock. The top and bottom elevations of layer 1 are 940 and 755 ft above mean sea level (amsl), respectively. This layer is very thick because upland areas exist in the eastern corners of the model; however, the maximum surface water feature elevation outside of these areas is only 795 ft. Since the minimum surface water feature elevation is 760 ft amsl, this thicker layer allows for all surface water features to be modeled in layer 1.

Whereas the hydrostratigraphic models included only the glacial sediments, the groundwater flow models initially were designed to include the bedrock units shown in Fig. G1. Therefore, the hydrostratigraphic model data and the bedrock elevation data from the LMBM (Feinstein *et al*., 2010) were compared in a spreadsheet in order to determine whether a particular node contained glacial deposits, bedrock, or both. If a node contained both glacial deposits and bedrock it was assigned to whichever unit had the greater volume of material in that node. If a node was in bedrock, it was assigned to a bedrock unit. Bedrock units are the Ancell Group, Prairie du Chien Group, and Cambrian sandstones (Fig. G1). Then the walls of the bedrock valley were further modified to correct for the lack of detail in the valley due to the large grid size of the LMBM. This was done by comparing the WCR data and mapping of the bedrock valley by Hooyer *et al*. (2008) in order to define the bedrock valley more accurately. The addition of the bedrock valley resulted in "losing" some of the high K units. The groundwater models have 10-16% sand and gravel.

Boundary Conditions

Initially, in early test models, head values were taken from the LMBM model along the four sides of the Outagamie County groundwater flow models in every layer and used to specify heads along the side boundaries. However, all six models had very poor calibrations, with every head target simulated higher than the observed, up to a 350 ft difference. Comparison of the LMBM head values with elevations of local surface water features from topographic maps and the head targets indicated the head values from the LMBM were all too high. Additionally, Feinstein *et al*. (2010) indicated few calibration points in this area of Outagamie County.

Because there are insufficient data to set the lateral boundaries, the layer 1 lateral boundaries were based on the surface water features, interpolating head between them. These boundaries were then used in every layer of the model as vertical hydraulic gradient information was not available near the boundaries. It was also found that the basal boundary condition needed adjustment. Initially, the bottom boundary, at the base of layer 98, was a no-flow boundary set in the Precambrian bedrock; the lower most layer containing glacial deposits is 83. The model was initially run with all 98 layers active. In order to simulate only the glacial deposits, head values based on values computed by the model with a no-flow boundary in the Precambrian bedrock were then assigned to all bedrock nodes, which effectively moved the lower boundary to the top of the bedrock valley. However, boundary heads proved to be too high, producing a thousand feet of water mounding on the surface. Therefore, during calibration, PEST determined one head value to be used as the lower boundary condition set at the bedrock valley walls. The top layer (upper boundary condition) has a specified flux equal to the recharge rates. Two recharge zones were specified based on conclusions drawn by Hooyer *et al*. (2008) that regions with 50 ft or less of glacial sediment have more recharge. The initial recharge rate was assigned as 1 in/yr in zone 1 and 6.4 in/yr in zone 2 (Fig G2), following Hooyer *et al*. (2008). Initial head values were set to 850 ft amsl for all cells.

The River Package was used to simulate major surface water features in the model area and the Drain Package to simulate minor surface water features (Fig. G3). Initially, only major surface water features were simulated, but this did not move enough water as indicated by the mounds of water found over large areas of the model. This problem was alleviated by adding minor water features as drain cells. Surface water features were digitized from a Geographic Information System (GIS) coverage of surface waters in Wisconsin imported to Groundwater Vistas as a map. River cells were defined as either lakes/wetlands or streams. Each lake/wetland cell was assigned a length and width so as to encompass the entire surface area of the cell. All stream cells were assigned a length of 1,200 ft and a width between 30-50 or 100 ft, based on average stream widths from topographic maps. Drain cells were assigned a length and width so as to encompass the entire surface area of the cell. Thickness of the streambed and lakebed sediment was arbitrarily set to 1 ft for all river cells and the vertical hydraulic conductivity of the bed was assigned a value of 4.5 ft/day for all river and drain cells, the average measured value for sand deposits (Freeze and

Cherry, 1979), which are prevalent along the major surface water features in the area. Literature values were assigned since local K values for fluvial sand deposits were not available. Streambed and lakebed elevations were estimated from topographic maps.

Model Properties

Porosity values (Table G1) were taken from the literature, including consolidation testing data from Hooyer *et al*. (2008). Hydraulic conductivity (K) is the only parameter that is different among the six models, as each is based on a different hydrostratigraphic model. Three different zones of K were used, one zone for each of the glacial deposits (fine-grained lacustrine/till, sand, and gravel). Locations of the glacial deposit zones were from the selected hydrostratigraphic models. Initial values of K (Table G1) for the glacial deposits were taken from Hooyer et al. (2008).

Table G1. Porosity and initial hydraulic conductivity values for each of the six models. Note that K_x indicates horizontal hydraulic conductivity for both the x and y directions, and K_z vertical hydraulic conductivity.

Unit	Porosity	Kx (ft/day)	Kz (ft/day)
lacustrine/till	0.3	2.83E-02	2.83E-04
sand	0.2	4.54	0.45
gravel	0.2	70.9	7.09

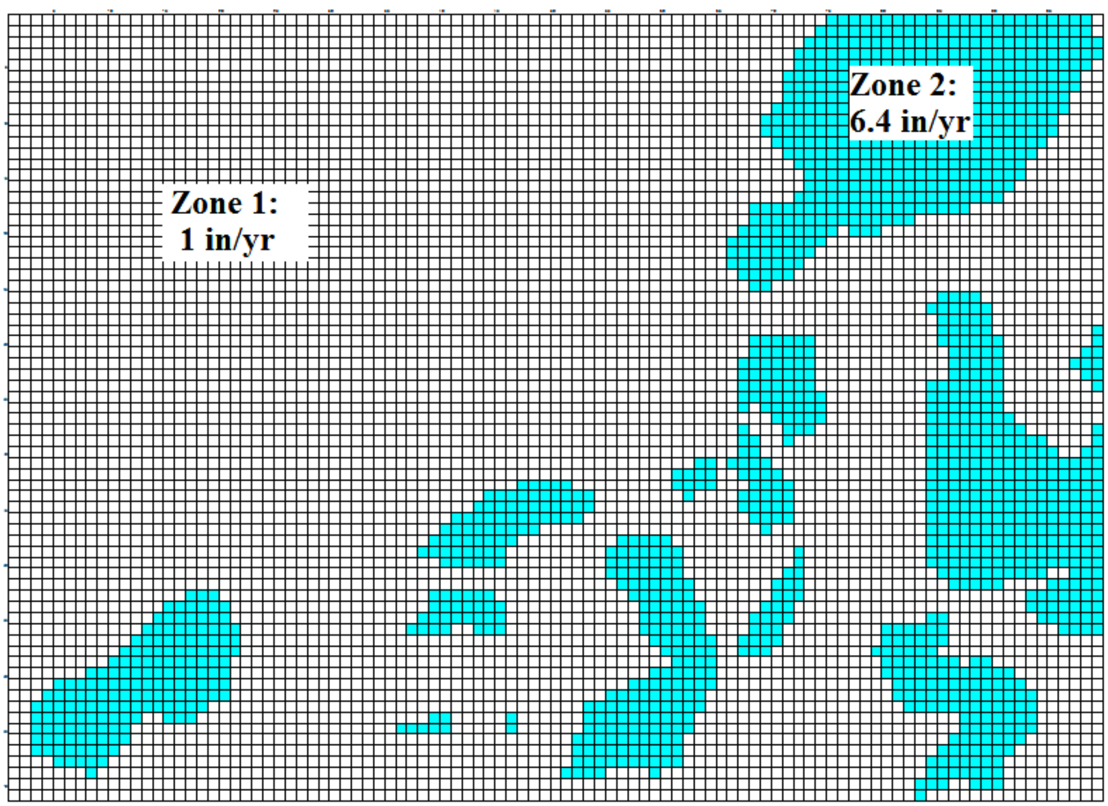

Figure G2. Initial estimates of recharge used in the groundwater flow models, taken from Hooyer *et al.* (2008).

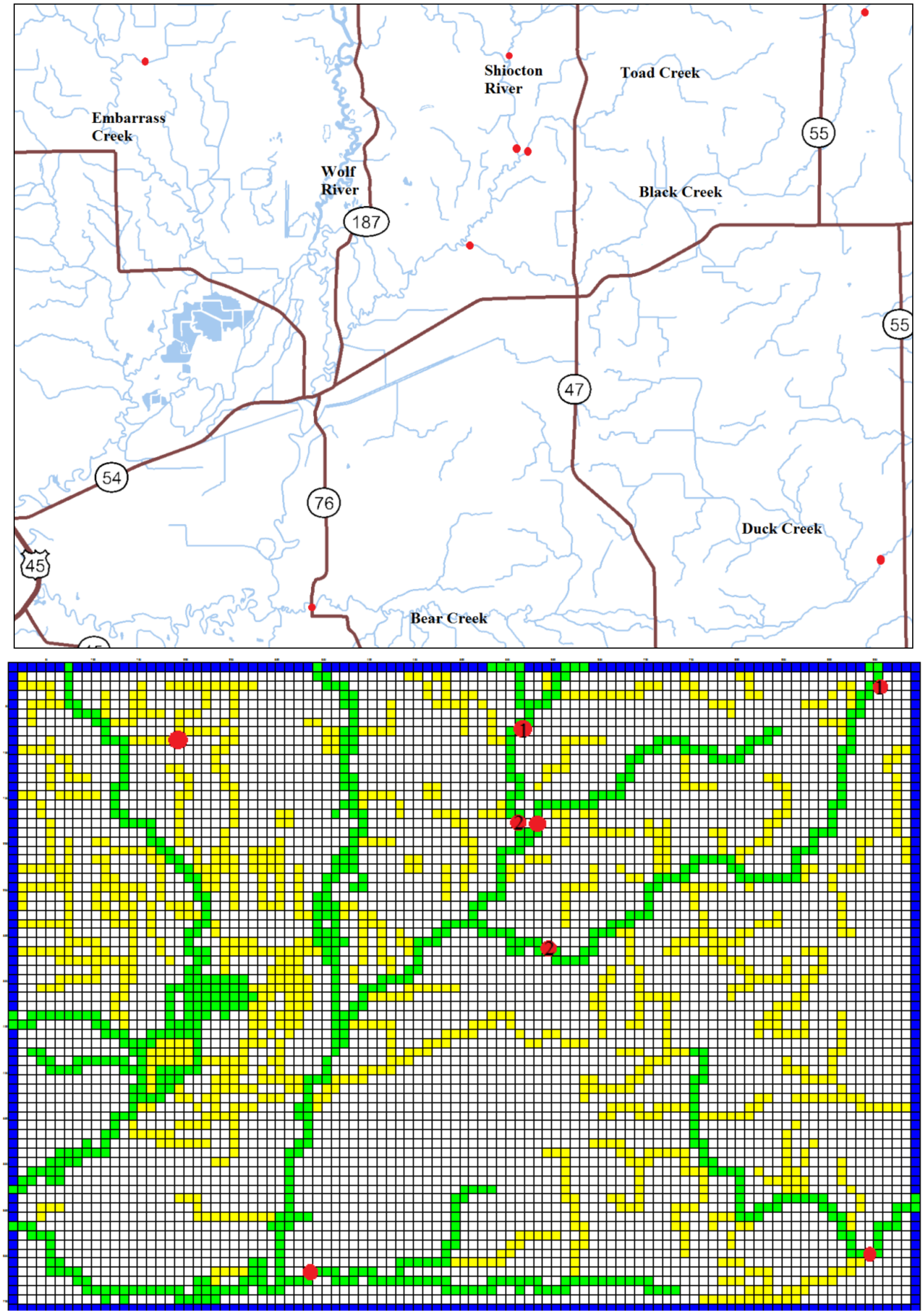

Figure G3. Location map of surface water features in the modeling area and layer 1 of the model showing the cells in the River Package (in green) and Drain Package (in yellow) used to simulate lakes, streams, and wetlands. Blue cells are specified head boundaries. Red dots indicate location of stream flux targets.

Calibration
Calibration of the six models was performed using the inverse code PEST (Doherty, 2004). PEST was used to determine optimal values of horizontal hydraulic conductivity (K_x), vertical hydraulic conductivity (K_z), recharge rates, and a constant head value for the bedrock nodes that formed the lower boundary. Note that initially PEST was run with five bedrock constant head zones, based on the bedrock units present in the study area (Fig. G1). However, this proved to be too many parameters for the available targets as PEST determined sand K to be lower than clay K and/or minimized recharge and maximized clay K for all six models.

Targets and Weights
Twenty head targets (Fig. G4) were used to calibrate the groundwater flow models, one of which was from a USGS long term monitoring well, nine from WCRs used in the geophysics site selection, and ten from Hooyer *et al*. (2008). The head targets were located throughout the model, with two targets in each of layers 1, 10, and 18, and one target each in layers 3, 4, 9, 15, 19, 21, 28, 29, 33, 34, 39, 44, 57, and 60. In addition to the head targets, six stream flux targets were used as a final check of the calibration (Fig. G3).

Weights were determined based on the credibility of the targets, with locations having lower measurement uncertainty receiving higher weights. The numbers were selected arbitrarily, with RS-18 values an order of magnitude higher than the WCRs. All RS-18 targets were given a weight of 10; all WCRs a weight of 1. The remaining targets from the Lorenz, Riehl, and USGS sites were given a weight of 5 as these targets were considered more uncertain due to their shallow locations (Lorenz/Riehl) or anomalously low head value (USGS).

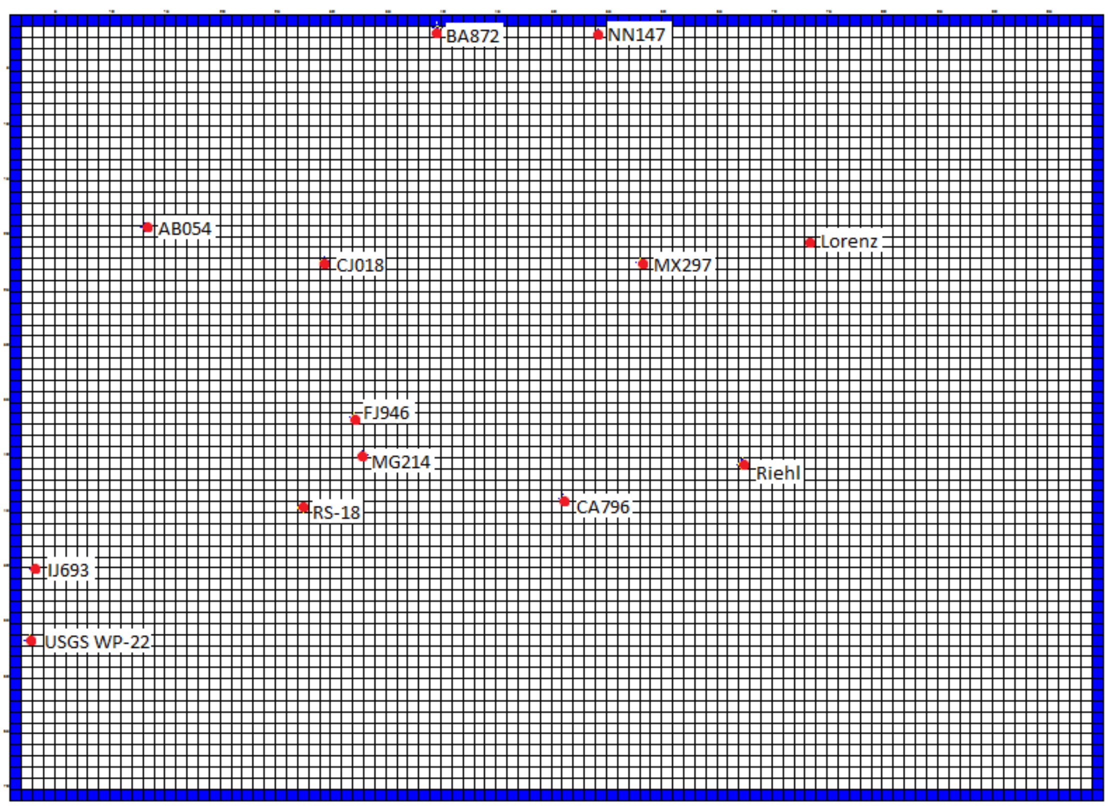

Figure G4. Location of head targets. Twenty targets are used from thirteen locations, with multiple targets at the RS-18 and Riehl sites. Note that targets labeled with two letters and three numbers are the WCRs.

Final Parameter Values
The final K_x and K_z values for the six models are shown in Table G2. The constant head value at the lower boundary was 760.28 in all six models. Except for zone 2 in model 10_7, which has a value of 6.4 in/yr, the value for both recharge zones is 1 in/yr for all six models. However, in model 10_7 the water table is above the land surface in the southwest corner of the model. The PEST determined value for recharge in zone 2 is less than that determined by Hooyer *et al*. (2008), who calculated the rate at only two sites and their value may not be representative of the entire area. Additionally, recharge results do not match the soil-water balance model recharge rates calculated by Hart & Schoephoester (2011), who estimated a mean recharge of 6.2 in/yr for Outagamie County, with some areas over 10 in/yr. Gebert *et al*. (2007) estimated mean recharge rates for Wisconsin based on streamflow measurements at gaging stations with long-term records. They estimated a mean recharge of 8.5 in/yr for all but the eastern edge of the modeling area, which they estimate at 1.6 in/yr.

Table G2. Final hydraulic conductivity values for each of the six models. K_x indicates horizontal hydraulic conductivity for both the x and y directions, and K_z vertical hydraulic conductivity.

Model:	**10_7**	**18_7**	**19_8**	**22_6**	**25_9**	**29_4**
Kx (ft/day)						
lacustrine/till	0.028	0.100	0.100	0.100	0.100	0.100
sand	4.535	4.536	4.536	4.538	4.536	4.535
gravel	70.866	70.866	70.866	70.866	70.866	70.866
Kz (ft/day)						
lacustrine/till	3.20E-03	1.11E-03	5.69E-04	1.55E-03	9.51E-04	5.60E-03
sand	0.454	0.454	0.454	0.454	0.454	0.454
gravel	7.087	7.087	7.087	7.087	7.087	7.087

In general, to improve calibration in cases where simulated heads are higher than observed values, recharge can be decreased or effective K (clay K for this site) can be increased to generate a better fit. For these six models, PEST determined the K_x of the clay to be 10^{-1} to 10^{-2} ft/day and K_z of the clay to be 10^{-3} to 10^{-4} ft/day. The determined K_z values are near the upper limit of the range of values of 10^{-3} to 10^{-7} ft/day determined by Hooyer *et al*. (2008); therefore, the recharge needed to be decreased in order to maintain measured values of K and have a better calibration. The difference in recharge rates between the soil-water balance model and the groundwater flow models could be due to the soil-water model accounting only for soil characteristics and not characteristics of glacial deposits. The WCRs indicated the presence of 0.5-1 ft of soil and 50-350 ft of glacial sediment throughout the modeled area. If recharge to the bedrock aquifers is more controlled by the thicker glacial sediment, the majority of which is fine-grained clay and till, lower recharge values would be expected. In addition to estimating mean recharge for Wisconsin based on streamflow measurements at long-term gaging stations, Gebert *et al*. (2007) also estimate mean recharge for low-flow partial-record stations in three major Wisconsin river basins. They found the overall basin estimate comparable to estimates based on data from the long-term streamflow-gaging stations, but found a wider range in recharge values (0.01 to 16.5 in/yr for the three studied basins). They note that it is likely this basin variability is typical in all the major drainage basins with calculated mean recharge from streamflow-gaging stations, and demonstrate this in a more recent report (Gebert *et al*., 2009). Their estimate for the entire Wolf River Basin, which covers approximately 3,690 mi^2, is 8.5 in/yr. However, low-flow partial record analysis determined a range of 0.1 to 34.4 in/yr in the Wolf River Basin. Furthermore, available records in the eastern half of the study area ranged from 0.1 to 2.2 in/yr, indicating it is likely that lower recharge values may be representative of the entire study area.

Calibration Results

The calibrated models varied in their ability to match the head targets (Table G3, Fig. G5). Generally, the RS-18 head targets had the best fit for all of the models (Fig. G6), which is expected given these were weighted higher during calibration. The shallow targets (Lorenz/Riehl) had the largest range of simulated values, likely due to a thicker layer 1. The absolute residual mean (arm) was between 10.93 ft and 12.50 ft for all six models, which is less than the arm value of 25.21 ft reported for the LMBM. Additionally, the mass balance was within 0.6% for all six models.

Eight measurements of stream flux data used to check the PEST calibrations (Fig. G3, Table G3). These measurements were made under approximately baseflow conditions. Two measurements were made for both Black Creek and the Shiocton River, in order to calculate a flux for one reach. The ditch feeding into the Embarrass River and Duck Creek had no measurable flows. All but one model simulated losing streams for both of these locations. For locations with measurable flow, a flow was considered to be simulated correctly if it was within one order of magnitude of the observed, due to the uncertainty in streamflow measurements. For Black Creek and the Shiocton River three of the models correctly simulated both streams, two correctly simulated flows for one of the streams, and only model 10_7 failed to correctly simulate either measured flow. With the exception of model 19_8, flows were simulated correctly for Toad Creek. Only two of the models correctly simulated flows for Bear Creek. However, Bear Creek runs nearly parallel to the southern model boundary; thus simulated fluxes may be affected by the specified head boundary. Individually, every model matched at least three of the six stream fluxes, with two matching a fourth target and three of them matching a fifth target. Thus results of the stream flux check indicate the PEST calibrations are acceptable, and any of the six models are equally plausible representations of glacial Lake Oshkosh sediment. However, none of these are highly calibrated models; thus they should not be used for groundwater management in Outagamie County.

Table G3. Calibration statistics for all six models. Note that only the heads were used as calibration targets with PEST, the stream flux data were used to check the calibrations. Stream fluxes are in ft^3/d, with positive numbers for gaining streams and negative for losing. The Shiocton River and Black Creek were calculated for one reach from two stream flux measurements (measurement 1 was subtracted from measurement 2, see Fig. G3 for locations).

Model:		**10_7**	**18_7**	**19_8**	**22_6**	**25_9**	**29_4**
Head Targets							
Residual Mean (ft)		-10.37	-6.74	-6.80	-5.59	-5.80	-3.61
Absolute Residual Mean (ft)		12.50	11.94	11.31	12.12	10.93	11.99
Root Mean Squared Error (ft^2)		5044	4277	3977	4170	3673	4421
Minimum Residual (ft)		-39.33	-26.96	-32.17	-24.27	-30.12	-27.90
Maximum Residual (ft)		15.00	19.51	21.90	26.35	21.22	27.61
Stream Flux Calibration Check							
Duck Creek	No Flow	-1.49E+05	-6.54E+04	-9.11E+04	-4.65E+04	1.20E+04	-3.05E+03
Ditch-Embarrass	No Flow	-1.05E+05	-1.90E+04	-1.33E+05	-3.00E+04	-8.38E+04	-5.98E+04
Black Creek	5.66E+05	-1.25E+04	3.26E+04	-4.38E+04	6.00E+04	3.07E+05	2.30E+05
Shiocton River	-1.12E+05	8.54E+03	-2.04E+04	-4.41E+04	-1.44E+04	-1.97E+04	4.72E+03
Toad Creek	5.66E+04	2.82E+05	4.87E+04	-1.66E+04	2.13E+04	1.95E+04	1.25E+05
Bear Creek	3.76E+05	1.02E+05	-2.86E+04	-4.89E+04	-1.54E+04	-2.28E+04	3.58E+04

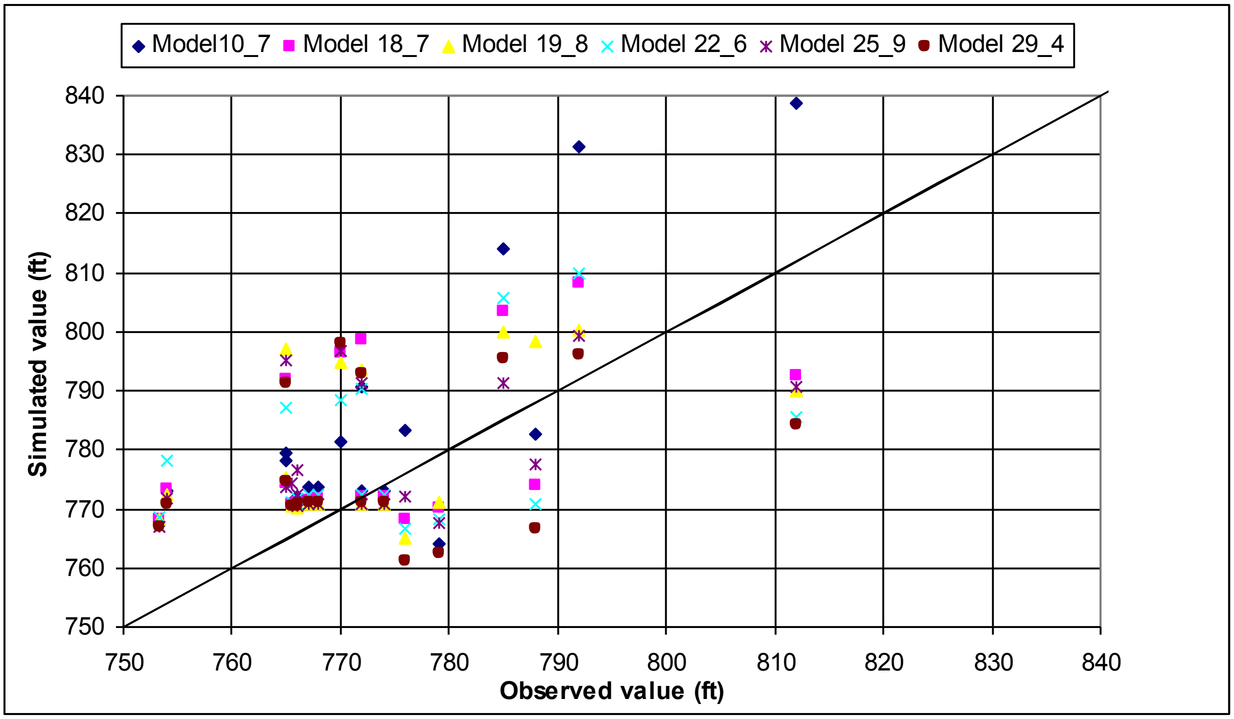

Figure G5. Observed verses simulated head values by model.

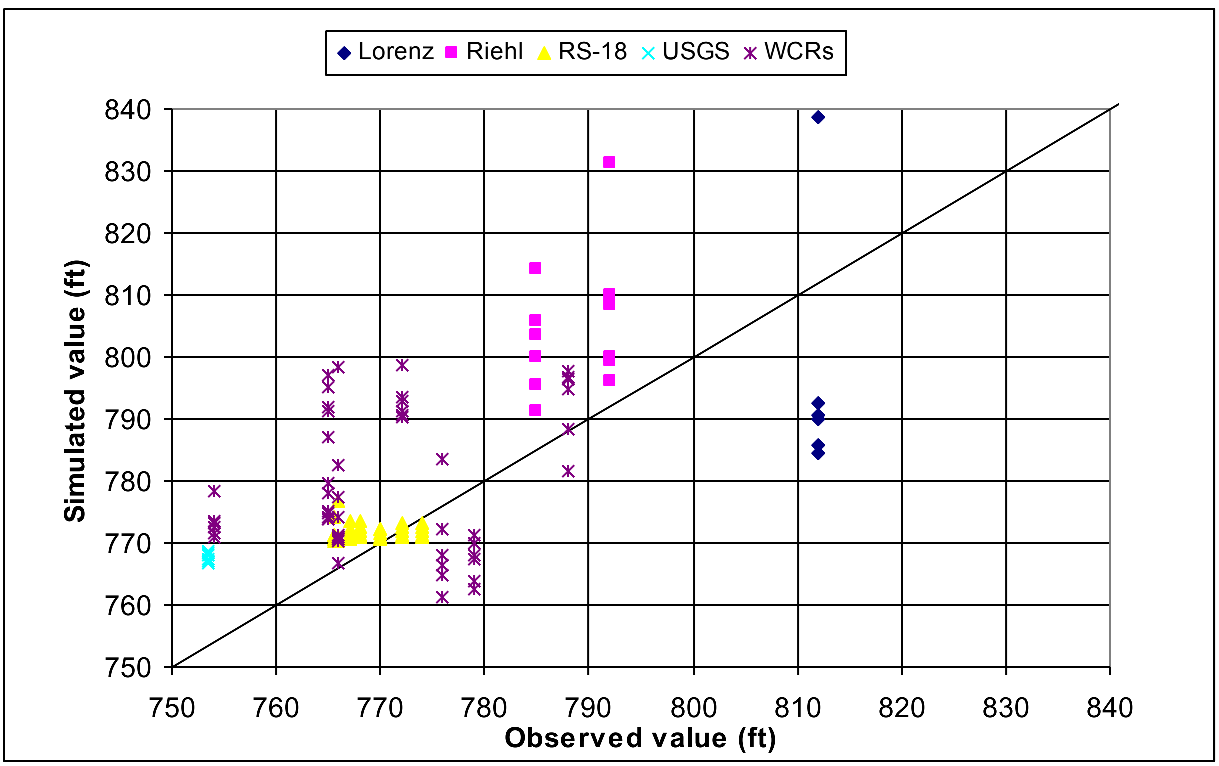

Figure G6. Observed verses simulated head values by target. Targets are grouped by location for the Lorenz, Riehl, RS-18, and USGS sites. All WCR target locations are grouped together. Note that the RS-18 targets have much better matches than the other sites.

MT3DMS
The groundwater flow models are run to steady-state and those heads are imported to MT3DMS (Zheng & Wang, 1999). A single stress period of 12,000 years (4.38*106 days) was selected for the MT3DMS simulations because this is the approximate length of time the entire model area was no longer glaciated and glacial Lake Oshkosh was fully drained and the area would likely start receiving modern day recharge values of $\delta^{18}O$. MT3DMS was run with an initial transport time step of 1,000 days with a 1.1 time-step multiplier and a maximum time step of 20,000 days, for a total of 241 transport time steps to reach the 12,000 years. The implicit finite difference solution with upstream weighting was used to solve for advection and dispersion.

Initial concentration of $\delta^{18}O$ for all cells was set at -30 ‰, a value typical of glacial-age water, and recharge set at -8‰, which represents modern day recharge values of $\delta^{18}O$ (Hooyer *et al.*, 2008). Dispersivity values of 100, 10^{-2}, and 10^{-4} ft were taken from Zheng and Bennett (2002) and assigned for longitudinal, transverse, and vertical dispersivity, respectively. Figures 11.4, 11.5, and 11.6 in Zheng and Bennett (2002) graphically display each of the dispersivities versus scale of observation, classifying the data by reliability. Values were selected from these figures, so that both the scale of observation and reliability were taken into account. It should be noted that dispersivity values are highly uncertain guesses at best.

Thirty $\delta^{18}O$ values from Hooyer et al. (2008) were used as an additional calibration check and to determine if the anomalous recent water found at depth could be explained by preferential flow paths. These targets are from four sites: Riehl, RS-18, RS-17, and RS-14 (Fig. 1). Each target is in a different layer, with the deepest located in layer 60.

The $\delta^{18}O$ values were matched the best by model 22_6 (Fig. G7, Table G4). Overall the best fit for all six models were the $\delta^{18}O$ values at RS-17 (Fig. G8). Figure G7 indicates that some of the models are allowing more recharge through certain areas of the bedrock valley so that the values are those of modern day recharge, while other models are restricting recharge so the values remain at the initial glacial water values. This difference is likely due to the presence of vertical preferential flow paths near the observation locations. Additionally, at seven of the targets modern $\delta^{18}O$ values were measured deep in the system while glacial values of $\delta^{18}O$ were measured in the shallow system. This suggests that present day recharge is being transported deep into the system via preferential flow paths. Overall, 76% of the simulated values at these anomalous seven targets for all six models are modern values; models 10_7 and 29_4 simulated modern $\delta^{18}O$ values for all seven targets.

The two models (18_7, 19_8) with the lowest percentage of particles exiting more than halfway vertically through the buried valley (Table 1) also had the most simulated $\delta^{18}O$ values remain at glacial values, indicating preferential flow is not occurring near the observations. Model 10_7 was the only model to have all simulated $\delta^{18}O$ values reach modern recharge values, indicating preferential flow is occurring near all observations. Also, as shown in Table 1, model 10_7 has a much higher percentage of particles exit the bedrock valley in fewer than 100 years (20.39%; all other models are less than 6%).

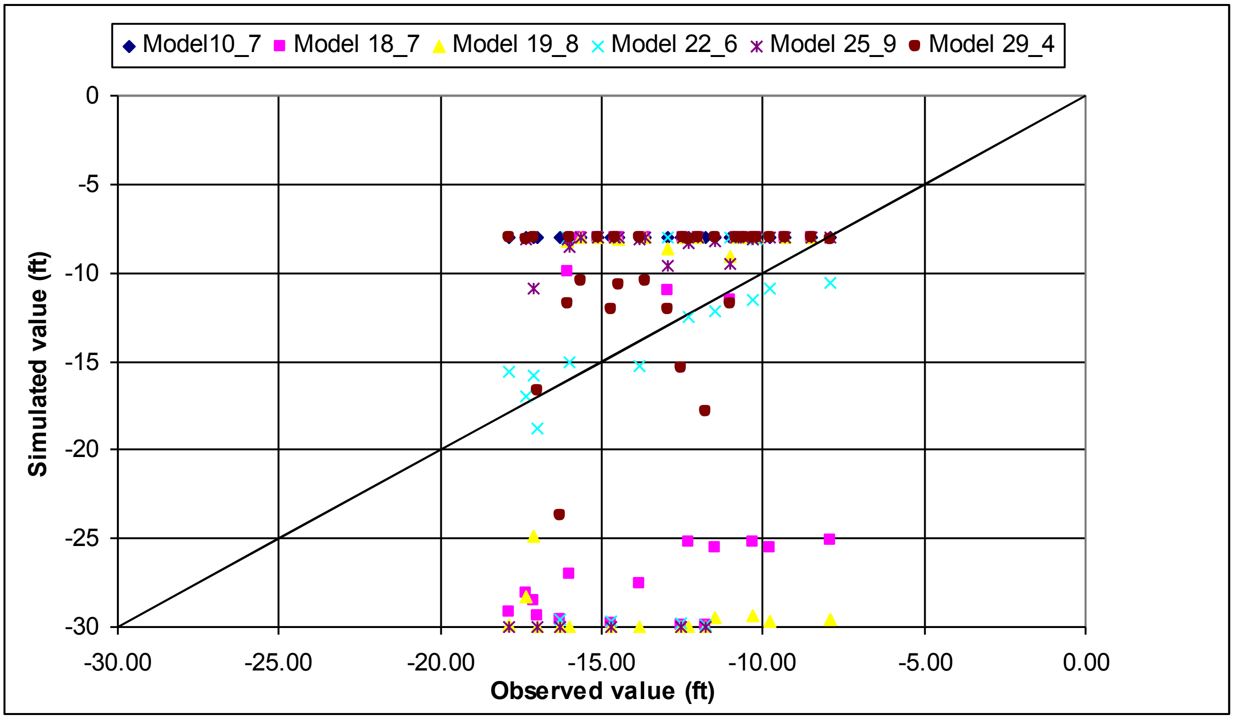

Figure G7. Observed verses simulated $\delta^{18}O$ values by model. Note the variation in models allowing more (e.g. 29_4) or less (e.g. 18_7) recharge to move through the deposits, likely due to the presence or lack of preferential flow paths near the observation locations, respectively. Also, model 22_6 matches the observed values much better than the other five models, indicated statistically in Table A4.1.

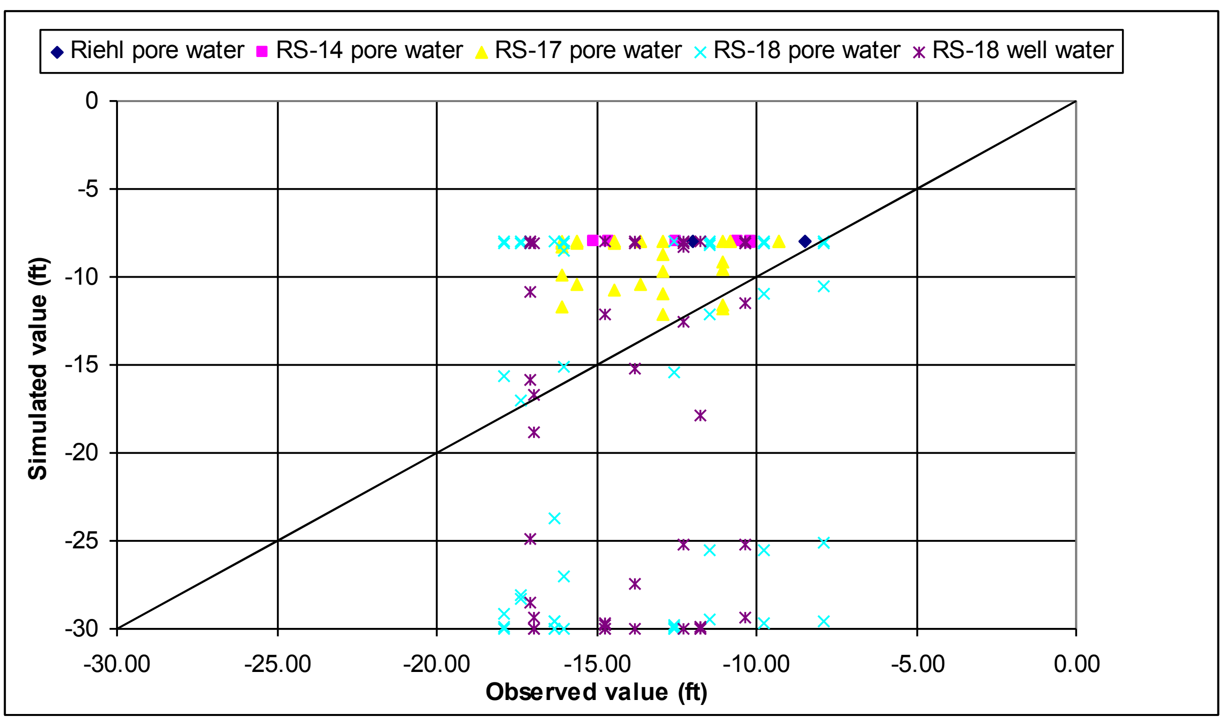

Figure G8. Observed verses simulated $\delta^{18}O$ values by location. Note that RS-18 is separated into pore and well water groups.

Table G4. Calibration statistics for all six models for the $\delta^{18}O$ values.

Model:	10_7	18_7	19_8	22_6	25_9	29_4
$\delta^{18}O$ Calibration Check						
Residual Mean (‰)	-5.16	5.00	5.65	-0.06	-0.47	-3.40
Absolute Residual Mean (‰)	5.17	8.97	10.00	4.90	6.46	4.56
Minimum Residual (‰)	-9.88	-7.63	-7.83	-8.07	-9.22	-10.26
Maximum Residual (‰)	0.09	18.11	21.69	18.12	18.24	7.44

APPENDIX H: Additional References in Appendices

de Vries, Luis Manuel, Carrerra, Jesus, Falivene, Oriol, Gratacós, Oscar, and Slooten, Luit Jan, 2009. Application of Multiple Point Geostatistics to Non-stationary Images. *Mathematical Geosciences*, vol. 41, p. 29-42.

Feinstein, D.T., Hunt, R.J., and Reeves, H.W., 2010, Regional groundwater-flow model of the Lake Michigan Basin in support of Great Lakes Basin water availability and use studies: U.S. Geological Survey Scientific Investigations Report 2010–5109, 379 p.

Freeze, R.A. and Cherry, J., 1979. *Groundwater*. Hemel Hempstead: Prentice Hall International, 660 p.

Gebert, Warren A., Radloff, Mandy J., Considine, Ellen J., and Kennedy, James L, 2007. Use of streamflow data to estimate base flow/ground-water recharge for Wisconsin. *Journal of the American Water Resources Association*, vol. 43, no. 1, p. 220-236.

Gebert, Warren A, Walker, John F., and Kennedy, James L., 2009. Estimating 1970-99 Average Annual Groundwater Recharge in Wisconsin Using Streamflow Data. U.S. Geological Survey Open-File Report 2009-1210, 118 p.

Hart, David and Schoephoester, Peter, 2011. Groundwater recharge in Calumet, Outagamie, and Winnebago Counties, Wisconsin, estimated by a GIS-based water-balance model: Wisconsin Geological and Natural History Survey, Open-file Report 2011-05, 26 p.

Ward, David S., Buss, David R., Mercer, James W., and Hughes, Shereen S., 1987. Evaluation of a groundwater corrective action at the Chem-Dyne Hazardous Waste Site using a telescopic mesh refinement modeling approach. *Water Resources Research*, vol. 23, no. 4, p. 603-617.

Zheng, Chunmiao and Bennett, Gordon D., 2002. Applied Contaminant Transport Modeling, John Wiley and Sons, Inc., New York, 621 p.